Role of Micropores in the Oxidative Dehydrogenation of Ethane on MoV(TeNb) Mixed Metal Oxides

An Honors Thesis for the Department of Chemical and Biological Engineering

Sopuruchukwu A. Ezenwa

Tufts University

May 2018

Thesis Committee: Professor P. Deshlahra (Chair), Professor K. Lee

"This new force, which was unknown until now, is common to organic and inorganic nature. I do not believe that this is a force entirely independent of the electrochemical affinities of matter; I believe, on the contrary, that it is only a new manifestation, but since we cannot see their connection and mutual dependence, it will be easier to designate it by a separate name. I will call this force catalytic force. Similarly, I will call the decomposition of bodies by this force ***catalysis****, as one designates the decomposition of bodies by chemical affinity analysis."*

— Jöns Jacob Berzelius

Translated from 'Some Ideas on a New Force
Which Acts in Organic Compounds', Annales chimie physiques, 1836

Abstract

Oxidative dehydrogenation (ODH) routes for the catalytic transformation of abundant light alkanes to higher value chemicals have the potential to overcome the current traditional processes and, in doing so, provide significant economic advantages and mitigate environmental concerns. Despite improved energy efficiency prospects, ODH based processes are yet to be fully implemented until catalysts with desired performance goals can be developed. MoV based mixed metal oxides with M1 phase are well known to produce high ethylene (C_2H_4) yields during ethane (C_2H_6) ODH at moderate reaction temperatures. Improvements of these materials have been limited by insufficient molecular level understandings of the nature of active sites and mechanistic origins of high selectivity. This experimental work examines the role of the micropores of these M1 phase oxides in controlling activity and selectivity. These micropores have similar sizes (0.4 nm) to C_2H_6, which hints at a well-matched fit that permits C_2H_6 access to active sites within the pores while cyclohexane (C_6H_{12}) remains restricted by size (0.6 nm) to external surface sites. Microporous MoVTeNbO and MoVO show significantly larger C_2H_6 to C_6H_{12} rate ratios than non-microporous vanadium oxides (VO_x/SiO_2), which indicates that nearly all C_2H_6 turnovers during ODH occur within the micropores. Activation enthalpy differences between C_2H_6 and C_6H_{12} on both MoVTeNbO and MoVO is observed to be lower than that on VO_x/SiO_2, which, in both MoV based oxides, is less reflective of the significant C-H bond strengths differences and more indicative of stabilization of C-H activations within micropores through van der Waals interactions. The trends of observed product selectivities during C_2H_6 and C_6H_{12} oxidations suggest that VO_x/SiO_2 and external surfaces of MoVTeNbO and MoVO provide similar relative preferences for C-H activation and O-insertion products, but the micropores in the latter oxides selectively promote C-H activation products. These experimental observations have been corroborated by density functional theory (DFT) studies which show that micropores stabilize desired C-H activation transition states and destabilize O-insertion reactions by steric hindrance to proximate C-O contact within the tightly confining concave pore walls. These detailed molecular level understandings provide important guidance to the development of improved selective oxidation catalysts for desired transformations that are limited by more favored but undesired reaction pathways.

Dedication

I would like to dedicate this Senior Honors Thesis to the memory of late Professor Jerry Meldon. He was an advisor, mentor and guiding force for my first three years at Tufts, but passed away in summer of 2017. He will be always remembered through the strong positive impact he left on me as well as on many other students, staff and faculty.

Acknowledgements

I would like to thank Dr. Leela Annamalai for her assistance with parts of my senior thesis project, not limited to but including catalyst synthesis and characterization, equipment training, and data analysis. I also thank Yilang Liu for his computational work that complemented this thesis work.

In addition, I thank Professor Kyongbum Lee for being on my thesis committee as well as providing helpful feedback and insights. I acknowledge our collaborators, Prof. Steve L. Suib and Yanliu Dang, for their assistance with the MoV(TeNb)O micropore volume and surface area measurements.

Finally, I am most grateful to my research advisor, Prof. Prashant Deshlahra, for his close mentorship and guidance throughout this project as well as during my entire time in his lab.

I acknowledge the following funding sources that were utilized one way or the other in this project: Tufts Faculty Research Fund, Tufts Collaborates Seed Grant, Tufts ChBE Undergraduate Summer Research Scholarship, XSEDE Computational Resources and Tufts High Performance Computing.

1. Introduction

1.1 *Motivation*

The recent shale gas boom has led to the increased production of light alkanes—mostly methane (CH_4), ethane (C_2H_6), and propane (C_3H_8)—in addition to an elevated flaring of the excess natural gas produced. Efficient and selective conversions of these carbon sources to useful chemicals and fuels through catalytic means are highly desired and could provide significant benefits to the chemical industry because of economic advantages and simultaneously alleviate environmental concerns.[1] Ethylene (C_2H_4), one of the most important industrial chemical feedstock, is currently produced mostly through steam cracking of naphtha or C_2H_6 and to a lesser extent through fluid-catalytic-cracking and trial catalytic dehydrogenation means as a result of the present superior economics of the steam cracking process.[2-3]

Oxidative dehydrogenation (ODH) of light alkanes, in contrast to endothermic cracking and dehydrogenation processes, provides an overall exothermic and energy-efficient route to the production of the corresponding alkenes.[4] Although ODH based processes provide improved energy efficiency and process simplicity, these incentives are yet to fully convince the major companies to switch over from the industry standard of steam cracking to ODH processes until better yields can be achieved.[2] Current minimum performance goals of 95% selectivity to C_2H_4 at greater than 60% conversion of C_2H_6 are suggested to be attainable by ODH processes to compete with the traditional steam cracking.[1]

1.2 *Background*

Oxidative Dehydrogenation of ethane, most commonly, involves the activation and subsequent reaction of the C_2H_6 and oxygen (O_2) reactants on reducible metal oxides

catalysts in a reduction-oxidation (redox) fashion that typically produces C_2H_4 in desirable primary C-H activation steps, and CO_x (x=1,2) in undesired secondary sequential or parallel oxygen (O)-insertion routes (Scheme 1), with water (H_2O) as a byproduct.[4] Typical to metal oxide catalysts, selectivity at higher conversions is limited by the facile sequential oxidations of the desired products to CO_x.[5]

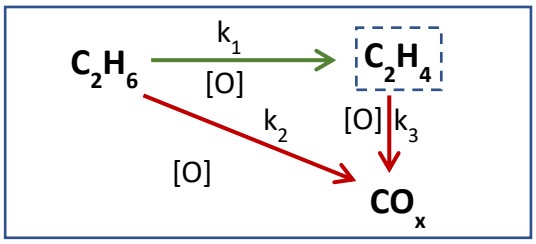

Scheme 1: Parallel and Sequential Routes in the Oxidative Dehydrogenation (ODH) of Ethane. k_1, k_2, and k_3 represent the pseudo-first order rate constants for C_2H_6 ODH, C_2H_6 combustion, and C_2H_4 combustion, respectively.

Of all the available C_2H_6 ODH catalysts, the orthorhombic M1 phase of mixed metal oxides of Mo, V, Te, and Nb has been shown to be the most selective to C_2H_4 at moderate reaction temperatures of 573-773 K.[6] Recent synthesis efforts succeeded in preparing M1 phase orthorhombic mixed metal oxides consisting of Mo and V only, which have also shown the same exceptionally high selectivity to C_2H_4.[7] The M1 phase of both the MoVTeNb and MoV oxides consists of layers of linked octahedral units of MO_6 (M=Mo, V) stacked along the [001] direction which forms pentagonal, hexagonal and heptagonal channels that can act as one-dimensional micropores in these layered solids.[7-8] The pentagonal and hexagonal pores are usually occupied by cations while the heptagonal pores stay partially open and could be accessible to small reactants.[7] The M1 phase of these MoV based catalysts have also been shown to be active and selective for the (amm)oxidation of propane to acrylonitrile or to acrylic acid and the oxidative dehydrogenation of propane.[6, 9-10]

The high activity of the MoVTeNb oxide catalyst has frequently been attributed to the (001) plane in the M1 crystal structure, [11-16] or the combination of specific crystal surface facets.[17] Within these (001) planes, V-oxo moieties were considered to be active sites.[14, 16] In addition, more reactive sites composed of Te-oxo species and generated surface O-radicals have also been proposed.[18-19] On the other hand, the high selectivity of these M1 phase oxides, has been generally attributed to "site isolation," which proposes that the active V sites spatially separated from each other prevent the over-oxidation of products on these sites.[20-21] The specific details on how these isolated sites selectively activate C-H bonds in alkanes and how over-oxidation of the alkene products on other isolated sites remain hypothetical. Common to most these, the identified activities and selectivity are proposed to occur on the external sites of the M1 phase MoVTeNb oxide.

Although, the presence of identical pores in M1 phase MoVTeNb and MoV oxides has been established through atomic-resolution microscopy,[10, 22] and the activation of C_2H_6 within micropores on the latter material has been proposed,[7, 23] the relevance of micropores to catalytic turnovers in the former has not been effectively studied. These pores possess diameters similar to kinetic diameter of C_2H_6 (0.4 nm)[7, 24] which can access them as determined by adsorption measurements. [7, 23, 25] In addition, the specific origin of the high selectivity to C_2H_4 during C_2H_6 ODH observed in these MoV based catalysts has not been addressed properly.

The role of pores in tuning reactivity and selectivity through steric restrictions on microporous zeolite materials has been identified,[26] and similar effects have been observed through the deposition of porous layers on existing non-porous metal oxides. [27] In bulk transition metal oxides, the specific role of micropores in selective oxidation reactions of alkanes is yet to be fully identified.

1.3 *Goal*

Within the past year, work done in the Deshlahra Lab has utilized well designed probe experiments and appropriate computational simulations to effectively demonstrate the influence of micropores of MoVTeNb oxide on the selective ODH of C_2H_6 to C_2H_4.[28] In this very recent work, we demonstrated, experimentally and computationally, that micropores selectively catalyze such reactions through stabilization of desirable C-H activation transition states and restriction of undesirable O-insertion steps.

Here, in this current work, insights used from our previous studies are used to reproduce the earlier observed catalytic effect of micropores of MoVTeNb oxide in addition to elucidating a similar role of heptagonal micropores in MoV oxide, another microporous M1 phase oxide. Experimentally derived rates for C_2H_6 and cyclohexane (C_6H_{12}) oxidative dehydrogenations on microporous MoVTeNbO and MoVO, as well as on different loadings of non-microporous VO_x/SiO_2, are used to further confirm the proposed role of micropores of molecular dimensions during selective alkane conversions. The bulky size of C_6H_{12} relative to C_2H_6 restricts its reactions to external surface of micropores, which are accessible by and responsible for most of the catalytic turnover of the latter, as indicated by the measured C_2H_6/C_6H_{12} activation rate ratios that are about two orders of magnitude higher on both MoV based oxides than the ratios on non-microporous supported VO_x.

We also show the dependence of C_2H_6 ODH turnover rates on micropore volume as well as C_6H_{12} reactions on external surface areas. In addition, in this work, we utilize relatively simpler and optimized experiments to determine apparent activation energies which when combined with product selectivity measurements, reinforces our theory that tight confinement of C_2H_6 within micropores stabilize C-H

activations via van der Waals interactions, but destabilize undesired O-insertion reactions through steric hindrance to close C-O contact within concave pore walls.

2. Experimental

2.1 *Synthesis of Metal Oxides*

Synthesis of bulk MoVTeNb and MoV oxides

The M1 phase MoVTeNb oxide (MoVTeNbO) was prepared using hydrothermal methods reported in literature.[29] All metal precursors were purchased from Sigma-Aldrich and used without further purification. MoVTeNbO was synthesized by first dissolving ammonium molybdate tetrahydrate $(NH_4)_6Mo_7O_{24}$ (52 mmol Mo in 67 ml H_2O)) at 353 K. Then vanadyl sulfate $VOSO_4$ (13 mmol V) and telluric acid $Te(OH)_6$ (12 mmol Te) were added to this solution under continuous stirring. Following this, the solution was cooled down to 313 K and dissolved ammonium niobate oxalate hydrate $(NH_4)[NbO(C_2O_4)_2(H_2O)_2] \cdot 3H_2O$ (6.5 mmol Nb in 33 ml H_2O) was added which led to an intial reaction mixture composition of 1:0.25:0.23:0.12 Mo:V:Te:Nb molar ratios. Nitrogen gas (Airgas, 99.99%) was bubbled to displace air for 5 minutes, and then this solution was then transferred to a 200 ml Teflon vessel contained within a stainless-steel autoclave and treated hydrothermally at 403K for 96 h in a preheated muffle furnace (Thermo Fisher). The obtained suspension was washed with deionized water, filtered and dried overnight in air in an oven maintained at 353 K for 16 h. Subsequently, the dried solids were heat treated in flowing He (50 ml min^{-1} Airgas, 99.999%) in a tube furnace ramped to 873 K at 0.083 K s^{-1} and held for 2 h.

The M1 phase of MoV oxide (MoVO) was prepared using a similar hydrothermal synthesis method as the MoVTeNbO earlier described and based on methods already reported.[30] To synthesize this orthorhombic MoVO, an aqueous solution of vanadyl sulfate $VOSO_4$ (0.05 mol L^{-1}) was added dropwise at ambient temperatue to a stirred aqueous solution of ammonium molybdate tetrahydrate $(NH_4)_6Mo_7O_{24}$ (0.2 mol L^{-1}). The initial reaction mixture contained Mo:V in a ratio of

4:1. Similar reaction and separation steps as MoVTeNb were carried out, except that the hydrothermal reaction occured at 348 K for 48 h. An additonal important purification step involving the dispersion of dried solids in oxalic acid (10 mmol L^{-1}) at 32 8K for 0.5 h was carried out with subsequent filtration, washing and overnight drying at 348 K. The dried solids were ground in a mortar and heat treated in a tube furnace ramped to 673 K at 0.167 K s^{-1} and held for 2 h.

Synthesis of silica supported vanadium oxides and bulk vanadia

Low weight loadings (1.5, 6.5, and 11 wt.%) of vanadium oxide supported on inert SiO_2 (VO_x/SiO_2) were prepared using standard incipient wet impregnation techniques found in literature.[31] All metal precursors were purchased from Sigma-Aldrich and used without further purification. The specific weights of the metal precursors used can be found in Table 1. A mixture of ammonium metavanadate NH_4VO_3 (1.96g; 99%) was dissolved in distilled water (1.5 ml) and added dropwise to nitric acid washed silica (2 g; Sigma-Aldrich Davisil Grade 633, ≥ 99%, 480 $m^2 g^{-1}$, 0.75 $cm^3 g^{-1}$). Then drying and calcination steps were carried out to obtain the solid catalyst.

A much higher loading (41 wt.%) of VO_x/SiO_2 was prepared using wet impregnation techniques. The vanadia precursor, ammonium metavanadate NH_4VO_3 (1.96g; 99%) was added to a stirred solution of oxalic acid (2.94 g; Sigma Aldrich, ≥ 99%) dissolved in deionized water (196 ml) at ambient temperature. Nitric acid washed SiO_2 powder (2.5 g; Sigma-Aldrich Davisil Grade 633, ≥ 99%, 480 $m^2 g^{-1}$) was added to the solution and the resulting mixture stirred at 373 K for 0.5 h to form a slurry that was dried overnight at 373 K in an oven and treated in flowing air (50 ml min^{-1}) in a tube furnace ramped to 873K at 0.083 K s^{-1} and held for 6h.

Bulk oxides of vanadia were synthesized using thermal decomposition of the NH_4VO_3 metal precursor (5g; 99%) in air at 773 K for 3h.[32]

Table 1. Weights of metal precursors used for the synthesis of loadings of VO_x/SiO_2

Mass of ammonium metavanadate NH_4VO_3 (mg)	Mass of Oxalic acid (mg)	Vanadia (VO_x) wt. % from ICP-AES	Theoretical surface densities V/nm^2
45.4	70.5	1.5	0.21
229.9	354.4	6.5	0.96
461.4	709.2	11	1.71
1960	2940	41	9.40

2.2 *Catalyst Characterization*

The MoVTeNbO catalyst obtained were characterized using powder X-ray diffraction (XRD) measurements performed on a Rigaku SmartLab diffractometer using monochromatic Cu Kα radiation (1.542 Å wavelength) and scans of 0.05° step sizes. An inductively coupled plasma atomic emission spectrometer (ICP-AES, Leeman labs PS-1000) was used to determine the elemental compositions of the catalysts. Scanning electron microscopy (SEM) images recorded using a Zeiss Ultra 55 SEM microscope with an acceleration voltage of 5 kV were used to inspect the morphology of the MoVTeNb oxide. Bright field micrographs and high-resolution images of MoVTeNbO were obtained using a JEOL T20 transmission electron microscope (TEM). The surface area of both MoV(TeNb) oxide catalysts was determined from volumetric N_2 physisorption isotherms obtained at 77 K using a Quantachrome Autosorb iQ2 apparatus after degassing the pretreating the samples in flowing He at 573 K for 3 h. The adsorption isotherm measured in the range of 0.05–0.35 was analyzed with the Brunauer-Emmett-Teller (BET) theory[33] to determine external surface area of manually ground MoVO and MoVTeNbO catalysts. The total micropore volume was determined using analysis based on adsorption at the low relative partial pressure (P/P_0) of 0.002.[34]

2.3 ***Measurements of Rate and product selectivity during ODH reactions***

Finely ground catalyst samples were used with or without dilution with acid washed SiO_2 and pelleted to retain 106–180 μm aggregates (intrapellet SiO_2/catalyst = 2) that were held as vertical fixed beds (Scheme 2) on a porous quartz frit within a U-shaped quartz tube (1.0 cm I.D.). These samples (0.005–0.7 g) were preheated to reaction temperatures (588–733 K) in flowing He (Airgas, 99.999%) at 0.25 K s^{-1} and held at constant reaction temperatures using a resistive furnace (National Element) prior to the introduction of reactant mixtures. Temperatures were measured using a K-type thermocouple (Omega) placed within a dimple on the quartz reactor wall and controlled electronically (Watlow, EZ-ZONE). The gaseous reactants (Airgas 25% C_2H_6/He; 3 kPa and 25% O_2/He; 3 kPa) and diluent He (Airgas, 99.999%) were metered by electronic mass flow controllers (Porter 601 CV series II) and C_6H_{12} (99.9%, Sigma-Aldrich; 0.5 or 3 kPa) was introduced and vaporized into the O_2/He streams using a liquid syringe pump (Cole Parmer, Model 100). All process transfer lines were kept above 363 K to avoid condensation of reactants or products.

The concentrations of reactor effluents were measured by an online gas chromatograph (Agilent 7890B) using capillary columns HP-PLOT Q (30 mm × 0.32 mm × 20.00 μm) or HP-1MS (30 mm × 0.32 mm × 1.00 μm) to separate C_2H_6 or C_6H_{12} and their oxidation products, respectively, both of which are connected to a flame ionization detector. A simultaneous injection is also made into a carboxen-1000 packed column (10', 1/8" tube, 60/80 mesh) used to separate CO, CO_2, O_2 and HCHO for analysis with a connected thermal conductivity detector. C_2H_4, CH_3CHO, CO and CO_2 were the only products detected for C_2H_6 ODH. Cyclohexene (C_6H_{10}), adipic acid ($C_6H_{10}O_4$), cyclohexanone ($C_6H_{10}O$), cyclohexenol ($C_6H_{10}O$), benzene (C_6H_6), CO and

CO_2 were detected for C_6H_{12} ODH. Conversions and selectivity are reported on a carbon basis.

During single condition experiments, the mass of catalyst was varied with constant reactant flow rates (30 cm^3 min^{-1}) to keep conversions within the differential range (<10%). The oxidative dehydrogenation turnover rates are reported as the moles of C_2H_6 or C_6H_{12} molecules converted per mole of V in catalyst per second. Significant homogeneous C-H activations were ruled out through blank reactor measurements at highest temperature and pressures representative of kinetic measurements which gave negligible conversions for C_2H_6 (< 0.01%, 733 K, 3kPa C_2H_6, 3kPa O_2 30 cm^3 min^{-1}) and C_6H_{12} (< 0.1%, 648 K, 3kPa C_2H_6, 3kPa O_2 30 cm^3 min^{-1}). Similar measurements were carried out on silica packed reactors which showed negligible effects of support on the observed ODH turnover rates (<0.25%, 733 K, 3kPa C_2H_6, 3kPa O_2 30 cm^3 min^{-1}, 0.26g SiO_2)

Observed ODH rates on all supported as well as bulk VO_x decreased continuously with time on stream (7-12% and 2-30% decrease for C_2H_6 at 648 K and C_6H_{12} at 648 K during the initial 1 h; Fig. A1(a)). Initial rates on these catalysts were obtained by extrapolating observed rates gotten within the first hour to zero time on stream to account for catalyst deactivation. In contrast, measured rates on MoVTeNbO and MoVO samples exhibited an initial increase for C_2H_6, as reported in literature,[25] and initial decrease for C_6H_{12}, but were more stable than VO_x/SiO_2 at longer times. Thus, these initial rates were obtained by averaging the observed stabilized rates which usually occurred after the first 30 mins of catalyst on reactant stream. The observed time dependent decrease rates on VO_x/SiO_2 are possibly due to the agglomeration of VO_x domains as these were less severe for the higher loadings (11, 41 and 100wt.%).

The absence of external mass transfer was confirmed through space velocity experiments which did not show any significant change in rate beyond that observed from product inhibition or reactant depletion in the assumed differential mode. Intra-pellet dilutions of the MoVTeNbO, MoVO and 41wt.% VO_x/SiO_2 catalyst (Fig. A2) showed that the rates were independent of dilution beyond the batch variations in MoVTeNbO grinding and pressing procedures (<20%) potentially caused by unsystematic changes to crystallite sizes and pore blocking. Our previous work[28] has also demonstrated that C_2H_6 translations within the micropores are relatively unhindered. The barriers for such translations are much smaller (<10 kJ mol^{-1}) than C-H activation barriers referenced to the same adsorbed intermediate (172 kJ mol^{-1}).[28] In addition to these results, the independence of C_2H_6 ODH rates to varying crystallite sizes reported earlier[7] strongly suggest that we can rule out any intrapellet concentrations or temperature gradients and that the local concentrations and temperatures in the catalyst bed are similar to those of the surrounding fluid phase. Thus, the measured rates reported in this work are free of transport artifacts and reflect the intrinsic chemical reaction rates from true kinetic limitations on reactant activations.

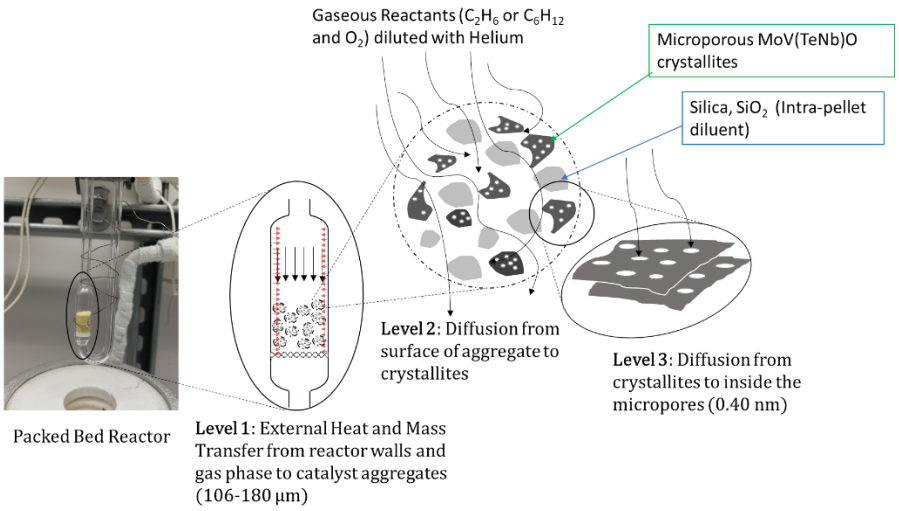

Scheme 2: Different scales of transport phenomena within our catalyst bed

3. Results and Discussion

3.1 *Characterization of MoVTeNbO, MoVO and VO_x/SiO_2*

Elemental composition

The composition of MoVTeNbO through ICP corresponds to $Mo_1V_{0.28}Te_{0.18}Nb_{0.25}$ stoichiometry, with significantly higher Te content than that used in our earlier study,[28] as a result of the longer synthesis time and lower synthesis temperature which facilitates the incorporation of Te in solution into the bulk oxide structure (Table A1). The absence of Te and Nb in the MoVO structure led to the reduced variability in reported elemental compositions of this oxide and thus the composition of MoVO used in this work was based off those and determined to be Mo_3V.[7-8, 23-25, 34] The specific loadings and theoretical surface densities of the VO_x/SiO_2 samples determined through ICP are summarized in Table 1.

Crystalline phase identification

The XRD patterns of MoVTeNbO and MoVO samples both showed an intense peak at a 2θ value of 22.1° (Fig. A3), with a d-spacing of 0.4 nm which corresponds to the distance between (001) planes in the M1 phase. Other possible minority phases (M2 and tetragonal M_5O_{14}) were not detected in our samples.[11]

Crystal morphology detection

The morphological structure of manually ground MoVTeNbO samples as observed through SEM, show plate and rod like structures characteristic of these materials (Fig. 1b). A similar morphology was observed on MoVO (Fig. 1a). High-resolution electron microscopy of the crystals through TEM also support that these materials are composed of the M1 phase. Though not explored in this work, more detailed atomic resolution investigations on similar materials through HAADF-STEM[21, 30, 35] and ABF-STEM,[8]

confirm the M1 phase as well as show the presence of heptagonal channels which could be partially occupied by metal cations.

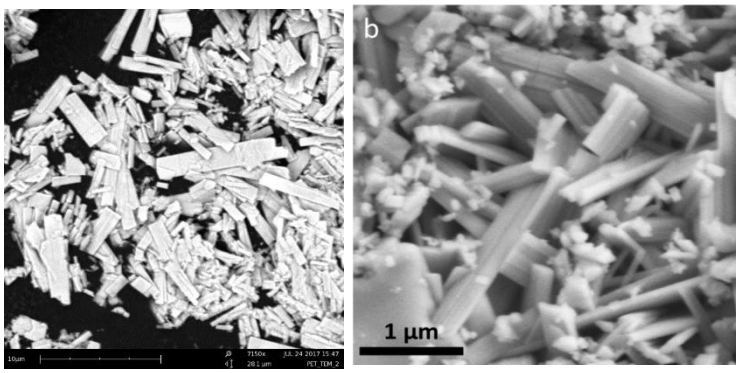

Figure 1: SEM Image for ground (a) MoVO (b) MoVTeNbO samples

Surface area and micropore volume quantification

The results from N_2 physisorption experiments on MoVTeNb and MoVO are shown in Figure 2. These adsorption isotherms showed a steep N_2 uptake at relative pressures (P/P_0) below 10^{-4} which reveals microporosity in these materials.

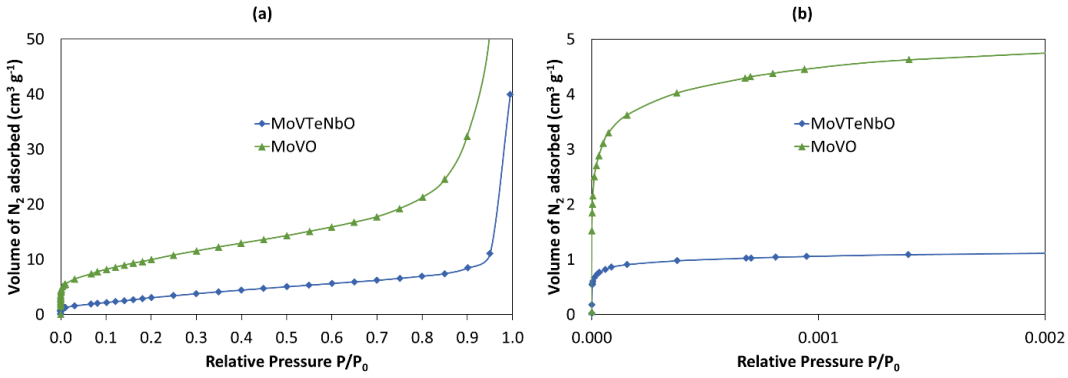

Figure 2: N_2 adsorption isotherm for the (a) entire P/P_0 range (b) low P/P_0 range at 77 K for ground MoVO and MoVTeNbO samples.

The micropore volume, V_{micro}, was calculated using the following equation:

$$V_{micro} = \frac{PV_{gas}}{RT} \times \frac{M}{\rho} \quad (1)$$

V_{gas} : N_2 uptake at 0.002 P/P_0 (at STP)
T and P: standard temperature (298 K) and pressure (1 atm)
ρ : density of liquid nitrogen (0.807 g cm^{-3})

M : molecular weight of liquid nitrogen 28 g mol^{-1}

The relevant micropore volumes, micropore wall areas, and external surface areas are shown in Table 2 (Area calculations shown in Appendix). The pore diameter has already been established to be about 0.4 nm.[7, 34]

Table 2: Micropore volumes, micropore wall areas and external surface area obtained by analyzing N_2 physisorption data on MoVTeNbO and MoVO

Catalyst	Micropore volume (10^{-3} cm^3 g^{-1})	Micropore wall area (m^2 g^{-1})	External Surface Area (m^2 g^{-1})
MoVTeNbO	1.58	15.7	11.8
MoVO	6.71	67.1	33.6

The measured micro pore volumes of MoV are similar to reported values,[30] but are about an order of magnitude different from theoretical values calculated for ethane adsorption.[7] These could be attributed to the loss of pore volume from dislocation of (001) plane during grinding or the partial occupation of metal cations within these pores. The micropore volume, as well as wall area, is about 5 times greater on MoVO when compared to MoVTeNbO, and this suggests that there is less occupancy of the pores by metal cations in the case of the former. In addition, the micropore wall areas are observed to be slightly higher than the corresponding external surface area, but remain within the same order of magnitude. These differences in micropore volumes and external surface areas between both MoV based oxides may have significant impacts to the reactivity of these samples during alkane ODH reactions.

Next, we utilize measured C_2H_6/C_6H_{12} rate ratios to estimate the relative contributions of these internal micropores and external surfaces to C_2H_6 ODH

3.2 *Measured C_2H_6/C_6H_{12} rate ratios on VO_x/SiO_2, MoVTeNbO and MoVO*

Rate Ratios on 41 wt.% VO_x/SiO_2 and MoV based oxides

Activation of C-H bonds in alkanes by lattice O-atoms on metal oxides surfaces (MO*) is the rate limiting step in these typical alkane reactions.[36] This H-abstraction step which

leaves behind reduced centers of oxygen vacancies (M*) or surface O-H groups (MOH*) is coupled to a fast and kinetically-irrelevant re-oxidation of these centers by gas phase O_2. The C_2H_6 and C_6H_{12} ODH rates are measured on microporous MoVTeNbO and MoVO as well as non-microporous VO_x/SiO_2 (41 wt.%). The latter has accessible O-atoms on their surfaces that are equally accessible to both C_2H_6 and C_6H_{12} molecules and thus do not provide any form of size restriction on these reactants. In contrast, on both MoV based catalysts, the heptagonal micropores may permit access to C_2H_6 molecules of similar kinetic diameter as their pore size (0.40 nm),[24] while restricting C_6H_{12} reactions to external surfaces on the basis of their larger kinetic diameter (0.6 nm)[37]. The accessibility of these external and internal sites is illustrated in Scheme 3.

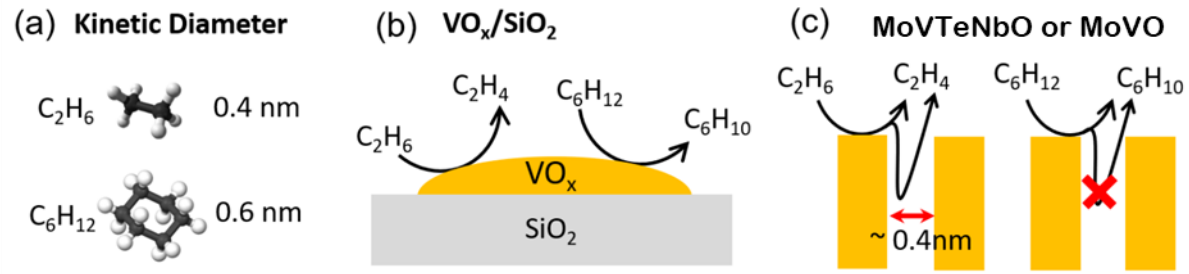

Scheme 3. (a) Kinetic diameters of reactants,[24,37] and accessibility of surface catalytic O-sites to C_2H_6 and C_6H_{12} reactants on (b) VO_x/SiO_2, and (c) MoVTeNbO or MoVO.

On VO_x/SiO_2, the ratio of the measured C_2H_6 and C_6H_{12} ODH rates represent the ratio of the C-H activation rates on the external sites present on this catalyst and are represented as ($r^{ext}_{C_2H_6}/r^{ext}_{C_6H_{12}}$):

$$\left(\frac{r_{C_2H_6}}{r_{C_6H_{12}}}\right)_{VO_x/SiO_2} = \frac{r^{ext}_{C_2H_6}}{r^{ext}_{C_6H_{12}}} \quad (2)$$

This representation of $r_{C_2H_6}/r_{C_6H_{12}}$ on VO_x/SiO_2 cancels out any uncertainties arising from the quantification of catalytically active sites by providing the same sites to both C_2H_6 and C_6H_{12} which have similar rate determining C-H activation steps. Thus, these values represent the relative difference in Gibbs free energies of these rate limiting steps

at identical active O-sites, and this depends on the nature, number and relative strength of the weakest C-H bonds in this molecule.[5, 36]

In both microporous MoVTeNbO and MoVO catalyst, the experimentally determined rate ratios will reflect an additional contribution ($r_{C_2H_6}^{pore}$) from internal pore sites which are accessible to only C_2H_6:

$$\left(\frac{r_{C_2H_6}}{r_{C_6H_{12}}}\right)_{MoVTeNbO\ or\ MoVO} = \frac{r_{C_2H_6}^{pore} + r_{C_2H_6}^{ext}}{r_{C_6H_{12}}^{ext}} \quad (3)$$

The measured rate ratios all three catalysts are shown in Figure 3. The C_2H_6 and C_6H_{12} turnover rates were measured at identical low conversions <8% (30 cm^3 min^{-1}, 3 kPa C_2H_6 or C_6H_{12}, 3 kPa O_2, 648 K) which represent rates that are independent of any significant product inhibition or reactant depletion and are devoid of any transport limitations as indicated earlier.

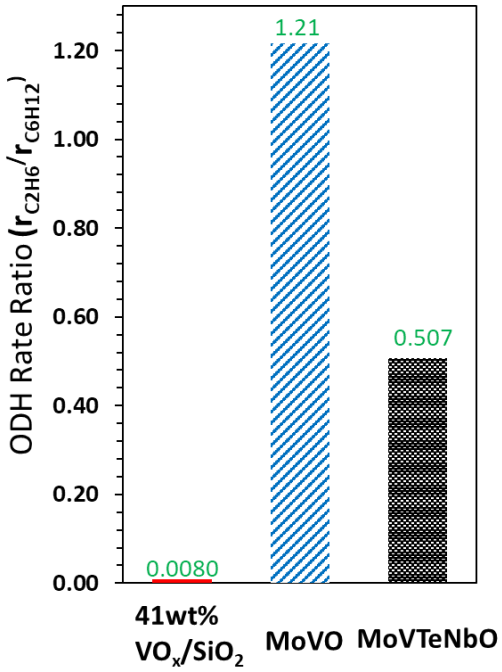

Figure 3: Measured C_2H_6/C_6H_{12} rate ratios on 41wt.% VO_x/SiO_2, MoVO and MoVTeNbO (648 K, 3 kPa C_2H_6 or C_6H_{12}, 3 kPa O_2, 30 cm^3 min^{-1}; Respective C_2H_6 conversions: 0.9%, 5% and 1.3%; Respective C_6H_{12} conversions 8%, 5% and 3%).

The observed rate ratios are much smaller on VO_x/SiO_2 than on both MoV based oxides. The low $r_{C_2H_6}/r_{C_6H_{12}}$ value (0.008) on VO_x/SiO_2 which is significantly lower than unity is because of the significant difference in bond strengths between C_2H_6 and C_6H_{12} (DFT derived bond dissociation enthalpy, BDE, 422 and 408 kJ mol^{-1} respectively; Appendix, Table A3). The stronger C-H bond in C_2H_6 relative to C_6H_{12} reflects its lower rate of activation.

On both MoVO and MoVTeNbO, however, the $r_{C_2H_6}/r_{C_6H_{12}}$ ratio is observed to be much closer to unity (1.21 and 0.507 respectively) despite the significant difference in bond strengths between C_2H_6 and C_6H_{12}. These ratios are about 150 and 65 times larger on MoVO and MoVTeNbO respectively, relative to VO_x/SiO_2, which suggests that the $r_{C_2H_6}^{pore}$ term in Equation 3 has two orders of magnitude greater contribution to the rate ratios than the ratios on only external surface that result from C-H bond strength differences. Therefore, the heptagonal micropores are responsible for most of C_2H_6 turnovers during ODH reactions.

These rate ratios obtained for MoVTeNbO are similar to those obtained in our earlier work which had MoVTeNbO with lower Te content (Table A1). When combined with our high rate ratio observed on MoVO, these suggest that Te atoms that partially occupy (Scheme A1) the micropores in MoVTeNbO, do not significantly affect the role of heptagonal pores in C_2H_6 turnovers.

Effect of VO_x surface density on Rate Ratios measured on VO_x/SiO_2

The 41wt.% VO_x/SiO_2 samples used in the previous section represent high V loadings (9.4 V/nm^2; Table 1) on the surface of the silica support and there are reports of different natures of surface active VO_x species present at different weight loadings.[32, 38] Irrespective of the loading weight percent, the active sites on these non-microporous

catalysts remain accessible to both C_2H_6 and C_6H_{12} and as such are regarded as external sites. Therefore, as stated earlier, representation of $r_{C_2H_6}/r_{C_6H_{12}}$ on different loadings of VO_x/SiO_2 (Eq. 2) cancels out any uncertainties arising from the quantification of catalytically active sites that are accessible to both reactants. Figure 4 shows the additional observed rate ratios on 1.5, 6.5, 11 wt.% loadings of VO_x on SiO_2 as well as on bulk unsupported V_2O_5. (Measured ODH rates on these loadings shown in Fig. A1.)

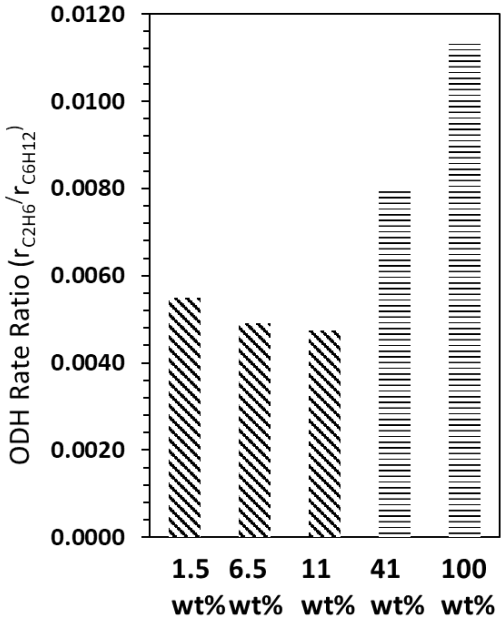

Figure 4: Measured C_2H_6/C_6H_{12} rate ratios on 1.5, 6.5, 11, 41wt% VO_x/SiO_2 and bulk V_2O_5, (648 K, 3 kPa C_2H_6 or C_6H_{12}, 3 kPa O_2, 30 cm^3 min^{-1}; Respective conversions C_2H_6: 0.04, 0.14, 0.53, 0.92, 0.47 %; C_6H_{12}: conversions 4, 5, 5, 8, 5 %).

These rate ratios on samples with different loadings of VO_x show values that are all much less than unity (0.005−0.011), which is consistent with the expected effect of stronger C-H bonds in C_2H_6 than in C_6H_{12}. The slightly higher values of these ratios on the samples with higher weight loadings (41 wt.% and 100 wt.%) than the samples with lower weight loadings potentially represent the different nature of active species reported on these weight loadings.[32] As the weight loadings increase, the surface densities of monovanadate ($O=V-(O)_x$) tend to decrease and those of polyvanadate

species (O=V−O−V=O) species and small V_2O_5 crystallites increase. Of these, the polyvanadate and V_2O_5 species are known to be more active for abstracting H-atoms from alkanes to form more stable surface OH bonds than monovanadate species.[32] The stronger hydrogen abstractors exhibit weaker discrimination between activation energies in C-H bonds of different strengths (C_2H_6 and C_6H_{12}), leading to higher rate ratios. These changes in bond-strength discrimination arise from changes to lateness of transition states predicted by Hammond's postulate[39] (Scheme 4).[5] According to this postulate, transition states for more exothermic reactions appear earlier along the reaction coordinate; the earlier transition states elongate the C-H bonds to lesser extents, which leads to lesser bond-strength discrimination. Nonetheless, these effects play only a minor role in measured rate rations because even the highest measured rate ratios on VO_x samples are much less than unity, which further confirms that the ratios near unity measured on microporous oxides must arise from the micropores.

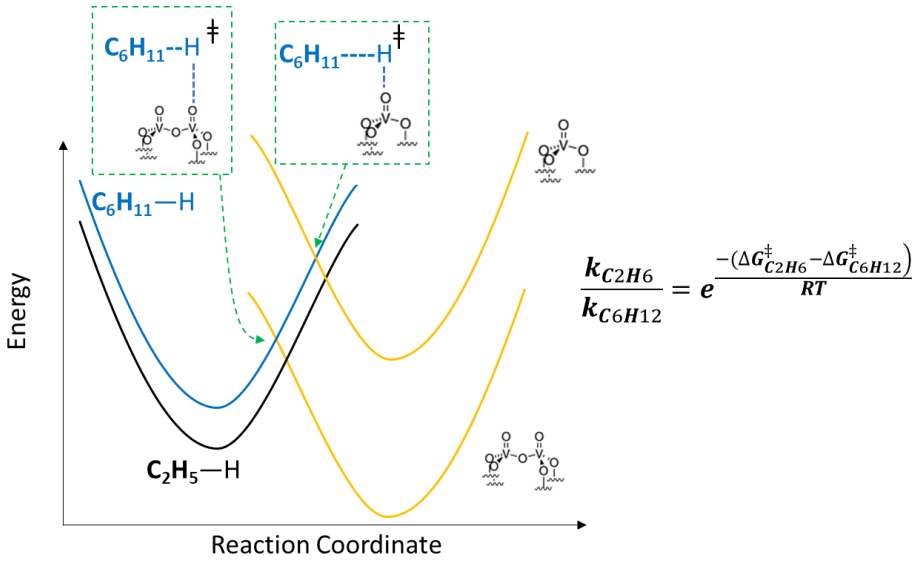

Scheme 4: Relative C-H activation transition states shown as overlaps of the parabolic potential energy surfaces of C-H bond dissociation and MO*-H bond formation. Stronger hydrogen abstractors (more negative H-atom addition energies (HAE)) and stronger C-H bonds (less positive bond dissociation energies (BDE)) are lower on this energy diagram. Stronger H-abstractors exhibit an earlier transition state which leads to lesser discrimination between C-H bonds of different strengths.

Thus, the difference in H-abstraction by active species cannot account for the observed high rate ratios in MoVTeNbO and MoVO which further suggests that most of C_2H_6 is activated within the pores during ODH.

Effects of micropore wall areas and external surface areas on rates measured on MoVTeNb and MoV oxides

Through the measured ODH rate ratios on MoVTeNbO, MoVO and VO_x/SiO_2, the relative magnitude of C_2H_6 turnover within micropores and C_6H_{12} turnover on external surfaces of both MoV based oxides has been established. It is observed that the C_2H_6 turnover rates are about 30 times larger on MoVO when compared to MoVTeNbO; similarly, the C_6H_{12} turnovers are about 13 times faster on MoVO relative to MoVTeNbO (Fig. 5)

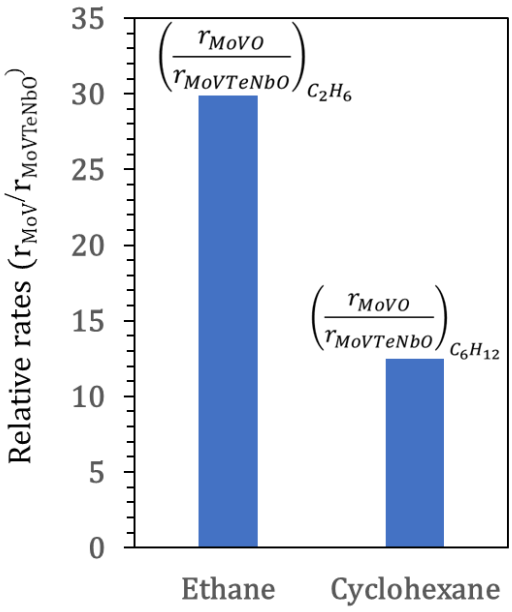

Figure 5: Measured relative C_2H_6 and C_6H_{12} ODH turnover rates on MoVO and MoVTeNbO (648 K, 3 kPa C_2H_6 or C_6H_{12}, 3 kPa O_2, 30 cm^3 min^{-1}; Respective C_2H_6 conversions: 5% and 1.3%; Respective C_6H_{12} conversions: 5% and 3%).

The relative magnitude between these rates could arise from uncertainties in quantifying the number of available catalytic active sites. Therefore, a ratio of rate ratios

will ensure that there is no specific need for such active site quantification. This relative $r_{C_2H_6}/r_{C_6H_{12}}$ ratio between MoVO and MoVTeNbO is expected to be similar to the relative micropore wall area (W.A.) to external surface area (S.A.) on both catalysts (Table 2):

$$\frac{\left(\frac{r_{C_2H_6}}{r_{C_6H_{12}}}\right)_{MoVO}}{\left(\frac{r_{C_2H_6}}{r_{C_6H_{12}}}\right)_{MoVTeNbO}} = \frac{\left(\frac{micropore\ wall\ area}{external\ surface\ area}\right)_{MoVO}}{\left(\frac{micropore\ wall\ area}{external\ surface\ area}\right)_{MoVTeNbO}} \quad (4)$$

The relative rate ratio (2.4) obtained is very similar in magnitude to the relative W.A. to S.A. ratio for both catalysts (1.5) which further confirms that C_2H_6 are activated within the pores while C_6H_{12} are restricted to external surfaces.

3.3 *Elementary steps in oxidative conversion of C_2H_6 and C_6H_{12}*

The oxidative conversion of C_2H_6 and C_6H_{12} on metal oxides typically form primary and secondary products as depicted in Scheme 5. A rate limiting C-H activation produces alkyl radicals that undergo rapid second C-H activations to form alkenes as ODH products. Parallel and sequential O-insertion reactions in the alkyl radicals and alkenes, ultimately form CO or CO_2.[38]

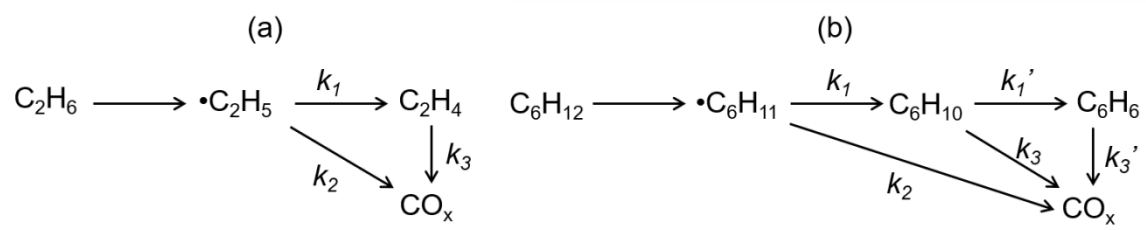

Scheme 5. Primary and secondary products formed in oxidative conversion of (a) C_2H_6 and (b) C_6H_{12}.

More detailed elementary steps for C_2H_6 ODH on metal oxides is shown in Scheme 4. These steps occur as typical Mars van Krevelen redox catalytic cycles.[40] The details of these steps have been described in our earlier work[28]. The cycle starts with the quasi-equilibrated adsorption of C_2H_6 in reactor feed or H_2O product on lattice O-atoms (MO*). The adsorbed C_2H_6 undergoes an irreversible C-H activation at an O-

atom to form a •C_2H_5 radical as well as surface OH species (MOH*). A second C-H activation of the latter radical forms C_2H_4 and as well as a second O-H pair (OH/MOH*). The first C-H activation remains kinetically relevant and the subsequent desorption of C_2H_4 and H_2O coupled with the sequence of irreversible re-oxidations of the reduced metal sites (M*) by O_2(g) complete the catalytic turnover. These steps as shown in Scheme 4 lead to an equation that describes the C_2H_6 ODH turnover rate per active metal center (M) as a function of the reactant and product pressures.[28]

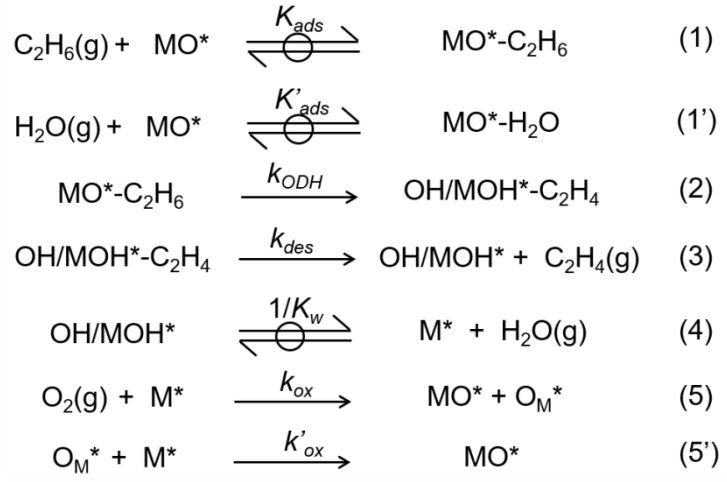

Scheme 6. Proposed elementary steps for C_2H_6 ODH at redox sites on both MoV based oxides and VO_x/SiO_2. M represents a metal center, which is interpreted as a V atom in both catalysts.

$$\frac{r_{ODH}}{[M]} = \frac{k_{ODH}K_{ads}P_{C_2H_6}}{1+K_{ads}P_{C_2H_6}+K'_{ads}P_{H_2O}+\frac{k_{ODH}K_{ads}P_{C_2H_6}}{2k_{ox}P_{O_2}}(1+K_wP_{H_2O})} \quad (5)$$

The denominator terms represent the ratio of concentrations of lattice oxygen (MO*), adsorbed ethane reactant (MO*-C_2H_6), adsorbed water product (MO*-H_2O), O-vacancies (M*), and surface hydroxyl species (OH/MOH*), in their respective order of appearance in the equation. The *k* and *K* values represent rate and equilibrium constants for the steps shown in Scheme 6. A very similar equation based on analogous elementary steps can be written for C_6H_{12} ODH through replacing C_2H_6 with C_6H_{12} as

well as adding an additional term ($K''_{ads}P_{C_6H_xO_y}$) in denominator to account for the possible adsorption of C_6H_{12} oxygenates at lattice oxygens.

$$\frac{r_{ODH}}{[M]} = \frac{k_{ODH}K_{ads}P_{C_6H_{12}}}{1+K_{ads}P_{C_6H_{12}}+K'_{ads}P_{H_2O}+K''_{ads}P_{C_6H_xO}+\frac{k_{ODH}K_{ads}P_{C_6H_{12}}}{2k_{ox}P_{O_2}}(1+K_wP_{H_2O})} \quad (6)$$

After the formation of radicals in the first step, parallel O-insertion reactions can occur to form oxygenates and thus limit selectivity to alkenes. These reactions are kinetically irrelevant as the first C-H activation dominates, but these oxygenates are included with the ODH alkene products in measured rates to accurately account for primary C-H activations.

Rigorous kinetic studies in our previous work[28] has shown the effect of product inhibition on turnover rates was studied by measuring the ODH rates as a function of C_2H_6 and C_6H_{12} conversions varied by changing the residence times at different reaction pressures. The decrease in C_2H_6 ODH rates with conversion (Fig. A4) was much weaker than the corresponding decrease in C_6H_{12} ODH rates (Fig. A5). Such differences in product inhibition may occur because the H_2O molecules formed in both reactions bind weakly to MO* sites at these temperatures,[4] but oxygenates formed in C_6H_{12} oxidations bind more strongly.[41] In addition, the same work[28] showed that C_2H_6 ODH rates increase linearly with C_2H_6 pressure and are independent in O_2 pressure (Fig. A6), which suggests that surface coverage of species represented by denominator terms in Equation 5 are much smaller than unity at relevant conditions due to weak alkane binding (K_{ads} << 1 kPa^{-1}) and rapid nature or re-oxidation steps (k_{ox}>> $k_{ODH}K_{ads}$). The C_6H_{12} ODH rates increased linearly with C_6H_{12} pressures at low pressures but exhibited sub-linearity at high C_6H_{12} pressures (Fig. A7). These nonlinear effects suggest that adsorbed C_6H_{12} derived species or reduced centers occupy significant fractions of surface sites at high C_6H_{12} pressure. These observations were

confirmed by the determination of the K_{ads} of both C_2H_6 and C_6H_{12} which were on average significantly less than unity across defined reaction temperature ranges on both MoVTeNbO and VO_x/SiO_2 (See Table A2).

With effects of product inhibition on ODH rates taken into consideration, appropriate reaction conditions were chosen to avoid the need for measurement of detailed effects of conversions and reactant pressures on measured rates. Low conversions of reactants (<5%) were ensured for all the rates reported henceforth to reflect ODH turnover rates at the conditions of reactor inlet free from product inhibition. In addition, low pressures of C_6H_{12} (0.5 kPa) and C_2H_6 (3 kPa) were used to select alkane pressures for which the denominator terms in equations 5 and 6 are insignificant. At these conditions, the rate equations 5 and 6 reduce to the following forms:

$$\frac{r_{ODH}}{[M]} \cong \frac{k_{ODH}K_{ads}P_{C_2H_6}}{1} \tag{7}$$

$$\frac{r_{ODH}}{[M]} \cong \frac{k_{ODH}K_{ads}P_{C_6H_{12}}}{1} \tag{8}$$

In addition, the effect of product inhibition on turnover rates was studied by measuring the ODH rates as a function of C_2H_6 and C_6H_{12} conversions varied by changing the residence times (Figure A8). These results confirm that our measured rates truly reflect the conditions at reactant inlet (zero conversion).

These rates were divided by C_2H_6 or C_6H_{12} pressures to obtain values of rate constants ($k_{ODH}K_{ads}$) according to Equations 7 and 8. These measured rate constants represent the Gibbs free energy of C-H activation transition state ($G^{\ddagger}$) relative to those of uncovered oxide surfaces (G_{MO*}) and gaseous C_2H_6 molecules ($G_{C_2H_{6(g)}}$):

$$k_{ODH}K_{ads} \sim e^{\frac{-\Delta G^{\ddagger}}{RT}} = e^{\frac{-(G^{\ddagger}-G_{MO*}-G_{C_2H_6(g)})}{RT}} \tag{9}$$

This equation is very similar for C_6H_{12} and next, we measure the differences in activation enthalpies between C_2H_6 and C_6H_{12} on both oxides to evaluate the role of micropores in stabilizing transition states for C_2H_6 activation.

3.4 *Role of micropores in C-H activation*

The Gibbs free energy change in Equation 9 reflects contributions from activation enthalpy and entropy ($\Delta G^{\ddagger} = \Delta H^{\ddagger} - T\Delta S^{\ddagger}$), which can be expressed in the form of the Eyring-Polanyi equation:[42-43]

$$ln\left(\frac{k_{ODH}K_{ads}h}{k_BT}\right) = \frac{\Delta S^{\ddagger}}{R} - \frac{\Delta H^{\ddagger}}{RT} \quad (10)$$

where, h and k_B represent the Planck and Boltzmann constants, respectively. Therefore, the apparent C-H activation enthalpies ($\Delta H^{\ddagger}$) can be estimated from a plot of the $ln(k_{ODH}K_{ads})$ values derived from measured rate constants (Table 3) for C_2H_6 and C_6H_{12} on VO_x/SiO_2, MoVTeNbO and MoVO as a function of reciprocal temperatures (Figs. 6(a)–(c)).

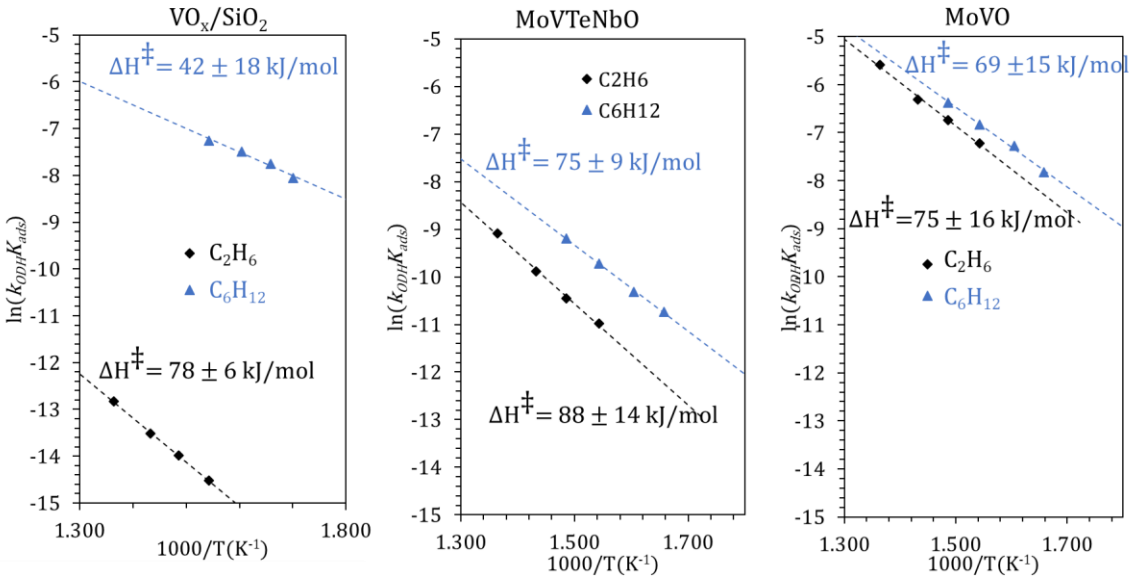

Figure 6. Measured ODH rate constants for activation of the C_2H_6 (black diamond) and C_6H_{12} (blue triangle) as a function of reciprocal temperature on VO_x/SiO_2 MoVTeNbO and MoVO. Dashed lines represent linear regression fits to form of equation 10. Uncertainty represents the 95% confidence interval on the estimation of the parameter in the linear regression.

Table 3. Estimated C-H activation rate constant for C_2H_6 and C_6H_{12} ODH obtained by dividing measured rates by $P_{C_2H_6}$ (3 kPa) and $P_{C_6H_{12}}$ (0.5 kPa) on VO_x/SiO_2, MoVTeNbO and MoVO.

Metal Oxide Catalyst	Temperature (K)	$k_{ODH}K_{ads}$ (10^{-5} $V^{-1}kPa^{-1}s^{-1}$)	Temperature (K)	$k_{ODH}K_{ads}$ (10^{-5} $V^{-1}kPa^{-1}s^{-1}$)
	C_2H_6 ODH		**C_6H_{12} ODH**	
41 wt% VO_x/SiO_2	648	0.050	588	31.7
	673	0.085	603	43.1
	698	0.136	623	55.9
	733	0.269	648	70.7
MoVTeNbO	648	1.69	603	2.17
	673	2.88	623	3.30
	698	5.07	648	6.02
	733	11.31	673	10.15
MoVO	648	73.4	603	39.8
	673	118.2	623	69.1
	698	180.9	648	108.0
	733	373.4	673	170.7

The C-H activation enthalpy of C_2H_6 (78 ± 6 kJ mol^{-1}) on VO_x/SiO_2 is significantly larger for than that of C_6H_{12} (42 ± 18 kJ mol^{-1}) which is consistent with the weaker C-H bond strength in the latter (Table A3). On both MoVTeNbO and MoVO, the C_6H_{12} activation enthalpies (75 ± 9 kJ mol-1 and 69 ± 15 kJ mol^{-1} respectively) are significantly higher than that on VO_x/SiO_2 which suggests a less reactive nature of O-atoms of both MoV based oxides due to their weaker H-abstraction strength. However, measured C_2H_6 activation enthalpies on MoVTeNbO (88 ± 14 kJ mol^{-1}) and MoVO (75 ± 16 kJ mol^{-1}) when compared to that on VO_x/SiO_2 do not seem to reflect these apparent weaker H-abstraction strengths of the O-atoms on these microporous MoV based oxides. In more quantitative terms of relative enthalpies between C_2H_6 and C_6H_{12} activations on these oxide catalysts, the activation enthalpy differences on MoV (6 kJ mol^{-1}) and MoVTeNbO (13 kJ mol^{-1}) are about 23-30 kJ lower than that observed on VO_x/SiO_2 (36 kJ mol^{-1}).

The rate ratios determined earlier in this work confirmed that most of C_2H_6 turnovers during ODH occur within the micropores (Fig. 3); therefore, the lower activation enthalpy difference between C_2H_6 and C_6H_{12} on both MoV and MoVTeNbO

is consistent with stabilization of C_2H_6 molecules by van der Waals (vdW) interactions with the micropore walls, as have been observed in zeotype materials which are porous as well.[44] Next the influence of micropores on the selectivity to ODH products will be probed.

3.5 *Influence of micropores on the selectivity to ODH products*

During rate measurements on the metal oxides, the product selectivity was measured (See Appendix for calculation details). Figure 7 shows the selectivity to C_2H_4 ($S_{C_2H_4}$) and other products in C_2H_6 oxidative conversion at a standard condition (30 $cm^3\,min^{-1}$) and as a function of C_2H_6 conversion ($X_{C_2H_6}$) for different C_2H_6 residence times (3 kPa C_2H_6 and 3 kPa O_2, 648 K). Both MoV and MoVTeNbO based catalysts showed a much higher selectivity to C_2H_4 (94 and 96% $S_{C_2H_4}$ at 7 and 2.5 % $X_{C_2H_6}$respectively; Fig. 7a) than VO_x/SiO_2 (49% $S_{C_2H_4}$ at 0.8% $X_{C_2H_6}$; Fig. 7a). In addition, the selectivity to C_2H_4 in both MoV based oxides stayed relatively the same over the 1-5% conversion range when compare to that on VO_x/SiO_2 which was much sensitive to increasing conversion (Fig. 7b), and these are consistent with the well-known selectivity trends on these materials.[6, 23, 45]

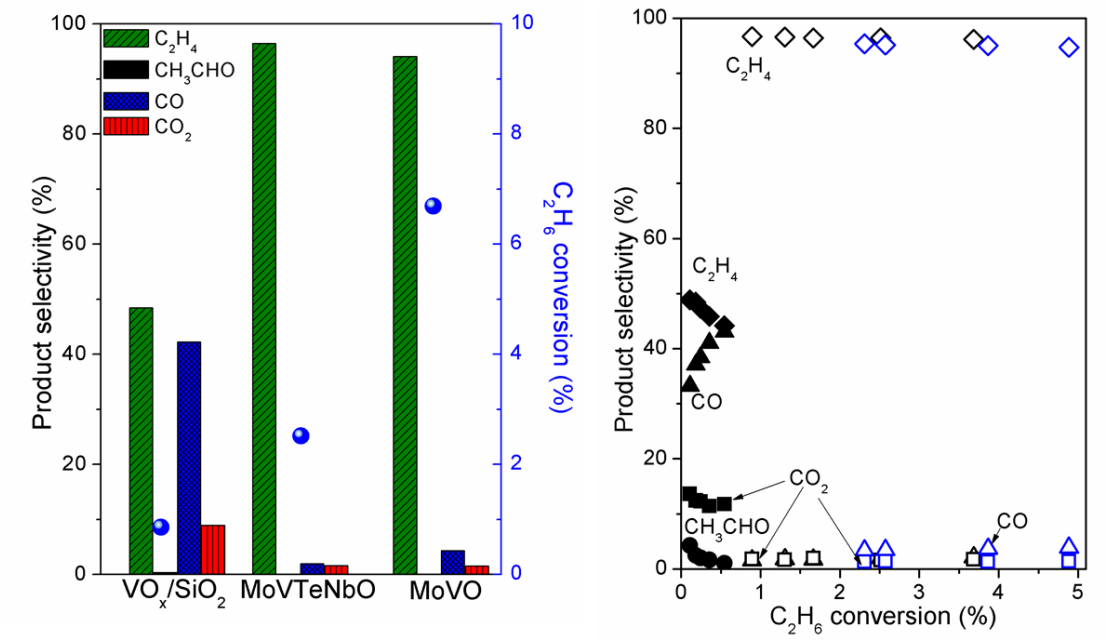

Figure 7. (a) C_2H_6 conversion and product selectivity at 30 cm^3 min^{-1} flow rate and (b) product selectivity as a function of C_2H_6 conversion on VO_x/SiO_2 (black closed symbols in b), MoVTeNbO (black open symbols in b), and MoVO (blue open symbols in b), at 648 K, 3 kPa C_2H_6, 3 kPa O_2.

However, measured product selectivity trends during C_6H_{12} oxidative conversion were similar on VO_x/SiO_2, MoVTeNbO, and MoVO at standard conditions ((30 cm^3 min^{-1} 0.5 kPa C_6H_{12} and 3kPa O_2, 648 K; Fig. 8a) which contrasted with the different trends observed during C_2H_6 conversion. In addition, the three C_6H_{12} product selectivity changed similarly with increasing conversion (Fig. 8b). These observed trends suggest that the nature of external surfaces of all three catalysts confer similar selectivity to oxidative dehydrogenation products (C_6H_{10} and C_6H_6) and that the high selectivity to C_2H_4 during C_2H_6 ODH on both MoVTeNbO and MoVO originates specifically from some property within the micropores.

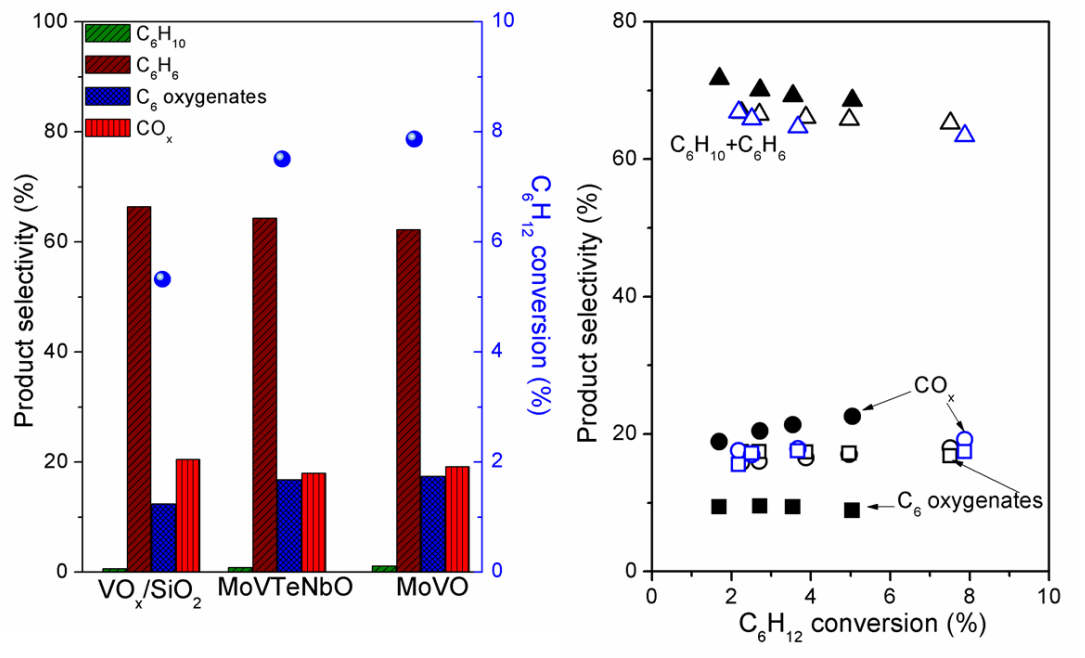

Figure 8. (a) C_6H_{12} conversion and product selectivity at 30 cm^3 min^{-1} flow rate and (b) product selectivity as a function of C_6H_{12} conversion on VO_x/SiO_2 (black closed symbols in b), MoVTeNbO (black open symbols in b), and MoVO (blue open symbols in b), at 648 K, 0.5 kPa C_6H_{12}, 3 kPa O_2.

Since the selectivity to all observed and possible C_2H_6 oxidative products have been accounted for (Fig 8b), Scheme 5 suggests that the selectivity to C_2H_4 on extrapolated to zero conversion represent the fraction of primary C-H activations that desirably branch towards C_2H_4 in contrast to those that go through a subsequent undesirable O-insertion to $\bullet C_2H_5$ radicals (near 100% $S_{C_2H_4}$ at zero $X_{C_2H_6}$ on both MoV based catalysts implies k_2/k_1 <<1 in Scheme 5). Likewise, the slope of selectivity versus conversion reflects the rates of secondary C_2H_4 combustion reactions relative to C_2H_4 formation (relatively small $-dS_{C_2H_4}/dX_{C_2H_6}$ implies small k_3/k_1). Thus, on MoVTeNbO and MoVO, the smaller rates of parallel and sequential O-insertion steps (k_2 and k_3 in Scheme 5) relative to the desirable dehydrogenation step (k_1), strongly suggest that the micropores hinder O-insertions during C_2H_6 turnovers within them.

Most of the results and logical deductions originating from this experimental work, have largely been supported by computational work done on appropriate

MoVTeNbO structural models (Fig. A9) using density functional theory in our previous work.[28] This study shows that hindrance to intimate C-O contact during potential O-insertion reactions inside the concave pore walls of MoVTeNbO appears to originate from tight confinement of C_2H_6 as well as C_2H_4 within these micropores. On the same note, the methods employed revealed that any such steric hindrances to the transfer of small H-atom from C_2H_6 to O-atoms within the pores are offset by the favorable benefits of vdW stabilization. Thus, the heptagonal pores enhance selectivity to alkenes by enhancing C-H activations while suppressing O-insertions through a synergistic blend of vdW interactions and steric effects which are summarized in Scheme 6.

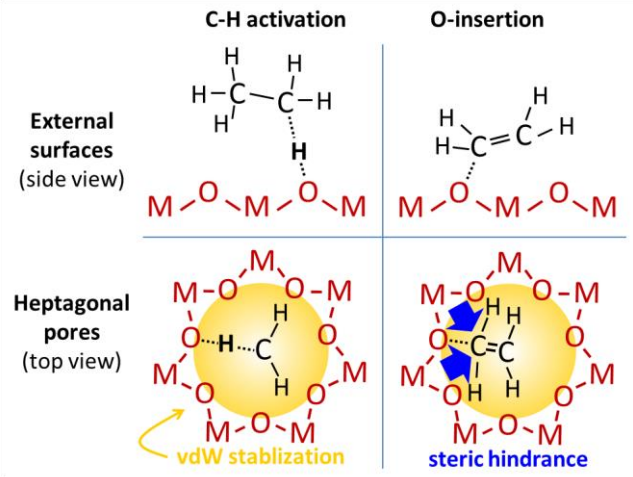

Scheme 6. Summary of influence of confinement in heptagonal pores on C-H activation and O-insertion steps.[28]

The detailed approach combined with the representative examples described in this study elucidate the important role of structural features of the complex M1 phase MoV based oxides in C_2H_6 ODH. This work further illustrates that the incorporation of Te and Nb into the matrix of these M1 phase materials do not appear to confer any significant activity or selectivity enhancements within them during C_2H_6 ODH, as have been reported,[7] although they might offer additional stability and more facile synthetic techniques. In addition, these insights demonstrate how micropores can tune desired

selectivity during catalytic transformations of molecules confined within them. The effects of confinement within pores of molecular dimensions have been established in zeotype materials, however, similar effects within micropores of bulk metal oxides were not completely identified. The current findings go beyond the early heuristic principle of site isolation in mixed oxides by providing a more detailed mechanistic connection to selectivity improvements in micropores. These molecular level understandings may provide important guidance to the development of improved selective oxidation catalysts through the incorporation of dispersion and steric forces as design criteria.

4. Conclusions and Future Work

The C_2H_6 to C_6H_{12} ODH rate ratios on non-microporous silica supported VO_x and bulk V_2O_5 and on microporous M1 phase MoVTeNbO and MoVO are used to study the role of micropores in selective ODH catalysis. The rate ratios on various loadings of VO_x/SiO_2 and bulk V_2O_5 are much smaller than unity, which is consistent with the weaker C-H bond in C_6H_{12}. The rate ratios on MoVTeNbO and MoVO, are significantly larger than those of VO_x, and are closer to unity which indicates high ODH turnovers of C_2H_6 within the micropores relative to external surfaces of these M1 phase materials.

Micropore volume and external surface area measurements from N_2 physisorption experiments confirm the microporosity of MoVTeNbO and MoVO; the relative values ratios of these volumes and areas on both oxides further corroborate the access of C_2H_6 molecules to active O-atoms within heptagonal pores and restriction of C_6H_{12} activations to external surface.

The measured activation enthalpy difference between C_2H_6 and C_6H_{12} is much lower (by ~25 kJ mol^{-1}) on both MoVO and MoVTeNbO than on VO_x/SiO_2 which suggest that C_2H_6 is stabilized by van der Waals interactions within the pores.

VO_x/SiO_2, MoVTeNbO, and MoVO show similar selectivities to C_6H_{12} oxidation products at similar reaction conditions and conversions, while selectivities to C_2H_6 oxidation products, are much higher on both MoV based oxides relative to that on VO_x/SiO_2. These trends suggest that external sites of all three oxides are similarly selective to C-H activation and O-insertion products, while the micropores are more selective to C-H activation products.

Furthermore, the calculated rate ratios, activation enthalpies, and observed product selectivity results obtained do not indicate any significant role of Te in activity and selectivity enhancements during C_2H_6 ODH on MoVTeNbO.

This work further confirms the results from previous experimental and computational work done in our lab, by showing that the role of micropores originates from the stabilization of desired C-H activation transition states and destabilization of O-insertion reactions by steric hindrance to proximate C-O contact within the tightly confining concave pore walls.

Ongoing investigations are probing such effects of micropores for propane (C_3H_8) ODH reactions on MoV, MoVTeNb and VOx/SiO_2 oxides. Some past work has attempted to passivate external surfaces of these MoV based M1 phase oxides and there are current plans in our lab to optimize this process to achieve the desired practical goal of further improved selectivity at higher conversions. Insights from the results of this work will be used as a guide to synthesize new materials for ODH reactions with tailored properties that confer similar effects of promoting desired transition states while suppressing undesired reaction pathways.

References

1. *The Changing Landscape of Hydrocarbon Feedstocks for Chemical Production*. Alper, J. ed.; National Academies Press: Washington, DC: **2016**.
2. Cavani, F.; Ballarini, N.; Cericola, A., Oxidative Dehydrogenation of Ethane and Propane: How Far from Commercial Implementation? *Catal. Today* **2007,** *127* (1), 113-131.
3. Gärtner, C. A.; Veen, A. C. v.; Lercher, J. A., Oxidative Dehydrogenation of Ethane: Common Principles and Mechanistic Aspects. *ChemCatChem* **2013,** *5* (11), 3196-3217.
4. Argyle, M. D.; Chen, K.; Bell, A. T.; Iglesia, E., Ethane Oxidative Dehydrogenation Pathways on Vanadium Oxide Catalysts. *J. Phys. Chem. B* **2002,** *106* (21), 5421-5427.
5. Deshlahra, P.; Iglesia, E., Reactivity and Selectivity Descriptors for the Activation of C-H Bonds in Hydrocarbons and Oxygenates on Metal Oxides. *J. Phys. Chem. C* **2016,** *120* (30), 16741-16760.
6. Nieto, J. L.; Botella, P.; Vázquez, M.; Dejoz, A., The Selective Oxidative Dehydrogenation of Ethane over Hydrothermally Synthesised MoVTeNb Catalysts. *Chem. Commun.* **2002,** (17), 1906-1907.
7. Ishikawa, S.; Ueda, W., Microporous Crystalline Mo-V Mixed Oxides for Selective Oxidations. *Catal. Sci. Technol.* **2016,** *6* (3), 617-629.
8. Trunschke, A.; Noack, J.; Trojanov, S.; Girgsdies, F.; Lunkenbein, T.; Pfeifer, V.; Hävecker, M.; Kube, P.; Sprung, C.; Rosowski, F.; Schlögl, R., The Impact of the Bulk Structure on Surface Dynamics of Complex Mo-V-based Oxide Catalysts. *ACS Catal.* **2017,** *7* (4), 3061-3071.
9. Oshihara, K.; Hisano, T.; Ueda, W., Catalytic Oxidative Activation of Light Alkanes Over Mo–V-Based Oxides Having Controlled Surface. *Top. Catal.* **2001,** *15* (2), 153-160.
10. Ueda, W.; Vitry, D.; Katou, T., Crystalline MoVO Based Complex Oxides as Selective Oxidation Catalysts of Propane. *Catal. Today* **2005,** *99* (1), 43-49.
11. DeSanto, P.; Buttrey, D. J.; Grasselli, R. K.; Lugmair, C. G.; Volpe, A. F.; Toby, B. H.; Vogt, T., Structural Aspects of the M1 and M2 Phases in MoVNbTeO Propane Ammoxidation Catalysts. *Z. Krist.*, **2004,** *219* (3), 152-165.
12. Grasselli, R. K.; Buttrey, D. J.; DeSanto, P.; Burrington, J. D.; Lugmair, C. G.; Volpe, A. F.; Weingand, T., Active Centers in Mo-V-Te-Nb-O_x (amm) Oxidation Catalysts. *Catal. Today* **2004,** *91*, 251-258.
13. Korovchenko, P.; Shiju, N. R.; Dozier, A. K.; Graham, U. M.; Guerrero-Pérez, M. O.; Guliants, V. V., M1 to M2 Phase Transformation and Phase Cooperation in Bulk Mixed Metal Mo-V-M-O (M=Te, Nb) Catalysts for Selective Ammoxidation of Propane. *Top. Catal.* **2008,** *50* (1), 43-51.
14. Li, X.; Buttrey, D. J.; Blom, D. A.; Vogt, T., Improvement of the Structural Model for the M1 Phase Mo-V-Te-Nb-O Propane (amm) Oxidation Catalyst. *Top. Catal.* **2011,** *54* (10-12), 614-626.
15. Shiju, N. R.; Liang, X.; Weimer, A. W.; Liang, C.; Dai, S.; Guliants, V. V., The Role of Surface Basal Planes of Layered Mixed Metal Oxides on Selective Transformation of Lower Alkanes: Propane Ammoxidation over Surface ab Planes of Mo-V-Te-Nb-O M1 Phase. *J. Am. Chem. Soc.* **2008,** *130* (18), 5850-5851.
16. Hävecker, M.; Wrabetz, S.; Kröhnert, J.; Csepei, L.-I.; d'Alnoncourt, R. N.; Kolen'ko, Y. V.; Girgsdies, F.; Schlögl, R.; Trunschke, A., Surface Chemistry of Phase-Pure M1 MoVTeNb Oxide During Operation in Selective Oxidation of Propane to Acrylic Acid. *J. Catal.* **2012,** *285* (1), 48-60.
17. Melzer, D.; Xu, P.; Hartmann, D.; Zhu, Y.; Browning, N. D.; Sanchez-Sanchez, M.; Lercher, J. A., Atomic-Scale Determination of Active Facets on the MoVTeNb Oxide M1 Phase and Their Intrinsic Catalytic Activity for Ethane Oxidative Dehydrogenation. *Angew. Chem. Int. Ed.* **2016,** *55* (31), 8873-8877.
18. Cheng, M.-J.; Goddard, W. A., The Mechanism of Alkane Selective Oxidation by the M1 phase of Mo-V-Nb-Te Mixed Metal Oxides: Suggestions for Improved Catalysts. *Top. Catal.* **2016,** *59* (17-18), 1506-1517.

19. Zhu, Y.; Sushko, P. V.; Melzer, D.; Jensen, E.; Kovarik, L.; Ophus, C.; Sanchez-Sanchez, M.; Lercher, J. A.; Browning, N. D., Formation of Oxygen Radical Sites on $MoVNbTeO_x$ by Cooperative Electron Redistribution. *J. Am. Chem. Soc.* **2017,** *139* (36), 12342-12345.
20. Callahan, J. L.; Grasselli, R. K., A selectivity factor in vapor-phase hydrocarbon oxidation catalysis. *AIChE Journal* **2004,** *9* (6), 755-760.
21. DeSanto, P.; Buttrey, D. J.; Grasselli, R. K.; Lugmair, C. G.; Volpe, A. F.; Toby, B. H.; Vogt, T., Structural Characterization of the Orthorhombic Phase M1 in MoVNbTeO Propane Ammoxidation Catalyst. *Top. Catal.* **2003,** *23* (1), 23-38.
22. Vogt, T.; Blom, D.; Jones, L.; Buttrey, D., ADF-STEM Imaging of Nascent Phases and Extended Disorder within the Mo-V-Nb-Te-O Catalyst System. *Top. Catal.* **2016,** *59* (17-18), 1489-1495.
23. Ishikawa, S.; Yi, X.; Murayama, T.; Ueda, W., Catalysis Field in Orthorhombic Mo_3VO_x Oxide Catalyst for the Selective Oxidation of Ethane, Propane and Acrolein. *Catal. Today* **2014,** *238*, 35-40.
24. Ishikawa, S.; Yi, X.; Murayama, T.; Ueda, W., Heptagonal Channel Micropore of Orthorhombic Mo_3VO_x as Catalysis Field for the Selective Oxidation of Ethane. *Appl. Catal., A* **2014,** *474*, 10-17.
25. Sadakane, M.; Ohmura, S.; Kodato, K.; Fujisawa, T.; Kato, K.; Shimidzu, K.-i.; Murayama, T.; Ueda, W., Redox Tunable Reversible Molecular Sieves: Orthorhombic Molybdenum Vanadium Oxide. *Chem. Commun.* **2011,** *47* (38), 10812-10814.
26. Yokoyama, H.; Kobayashi, H.; Hasegawa, J.-y.; Fukuoka, A., Selective Dehydration of Mannitol to Isomannide over Hβ Zeolite. *ACS Catal.* **2017,** *7* (7), 4828-4834.
27. Canlas, C. P.; Lu, J.; Ray, N. A.; Grosso-Giordano, N. A.; Lee, S.; Elam, J. W.; Winans, R. E.; Van Duyne, R. P.; Stair, P. C.; Notestein, J. M., Shape-Selective Sieving Layers on an Oxide Catalyst Surface. *Nat. Chem.* **2012,** *4* (12), 1030-1036.
28. Annamalai, L.; Liu, Y.; Ezenwa, S.; Dang, Y.; Suib, S. L.; Deshlahra, P., Influence of Tight Confinement on Selective Oxidative Dehydrogenation of Ethane on MoVTeNb Mixed Oxides. Manuscript submitted for publication, **2018.**
29. Sanfiz, A. C.; Hansen, T. W.; Girgsdies, F.; Timpe, O.; Rödel, E.; Ressler, T.; Trunschke, A.; Schlögl, R., Preparation of Phase-Pure M1 MoVTeNb Oxide Catalysts by Hydrothermal Synthesis-Influence of Reaction Parameters on Structure and Morphology. *Top. Catal.* **2008,** *50* (1-4), 19-32.
30. Konya, T.; Katou, T.; Murayama, T.; Ishikawa, S.; Sadakane, M.; Buttrey, D.; Ueda, W., An orthorhombic Mo3VOx catalyst most active for oxidative dehydrogenation of ethane among related complex metal oxides. *Catalysis Science & Technology* **2013,** *3* (2), 380-387.
31. Barman, S.; Maity, N.; Bhatte, K.; Ould-Chikh, S.; Dachwald, O.; Haeßner, C.; Saih, Y.; Abou-Hamad, E.; Llorens, I.; Hazemann, J.-L.; Köhler, K.; D' Elia, V.; Basset, J.-M., Single-Site VOx Moieties Generated on Silica by Surface Organometallic Chemistry: A Way To Enhance the Catalytic Activity in the Oxidative Dehydrogenation of Propane. *ACS Catalysis* **2016,** *6* (9), 5908-5921.
32. Khodakov, A.; Yang, J.; Su, S.; Iglesia, E.; Bell, A. T., Structure and properties of vanadium oxide-zirconia catalysts for propane oxidative dehydrogenation. *Journal of Catalysis* **1998,** *177* (2), 343-351.
33. Brunauer, S.; Emmett, P. H.; Teller, E., Adsorption of Gases in Multimolecular Layers. *Journal of the American Chemical Society* **1938,** *60* (2), 309-319.
34. Sadakane, M.; Kodato, K.; Kuranishi, T.; Nodasaka, Y.; Sugawara, K.; Sakaguchi, N.; Nagai, T.; Matsui, Y.; Ueda, W., Molybdenum-Vanadium-Based Molecular Sieves with Microchannels of Seven-Membered Rings of Corner-Sharing Metal Oxide Octahedra. *Angew. Chem. Int. Ed.* **2008,** *47* (13), 2493-2496.
35. Pyrz William , D.; Blom Douglas , A.; Vogt, T.; Buttrey Douglas , J., Direct Imaging of the MoVTeNbO M1 Phase Using An Aberration-Corrected High-Resolution Scanning Transmission Electron Microscope. *Angewandte Chemie International Edition* **2008,** *47* (15), 2788-2791.

36. Zboray, M.; Bell, A. T.; Iglesia, E., Role of C-H Bond Strength in the Rate and Selectivity of Oxidative Dehydrogenation of Alkanes. *J. Phys. Chem. C* **2009,** *113* (28), 12380-12386.
37. Muller, J. A.; Conner, W. C., Cyclohexane in ZSM 5. 1. FTIR and X-ray Studies. *J. Phys. Chem.* **1993,** *97* (7), 1451-1454.
38. Argyle, M. D.; Chen, K.; Bell, A. T.; Iglesia, E., Effect of Catalyst Structure on Oxidative Dehydrogenation of Ethane and Propane on Alumina-Supported Vanadia. *J. Catal.* **2002,** *208* (1), 139-149.
39. Hammond, G. S., A Correlation of Reaction Rates. *Journal of the American Chemical Society* **1955,** *77* (2), 334-338.
40. Mars, P.; Van Krevelen, D. W., Oxidations Carried Out by Means of Vanadium Oxide Catalysts. *Chem. Eng. Sci.* **1954,** *3*, 41-59.
41. Birky, T. W.; Kozlowski, J. T.; Davis, R. J., Isotopic Transient Analysis of the Ethanol Coupling Reaction Over Magnesia. *J. Catal.* **2013,** *298*, 130-137.
42. Eyring, H., The Activated Complex in Chemical Reactions. *J. Chem. Phys.* **1935,** *3* (2), 107-115.
43. Evans, M. G.; Polanyi, M., Some Applications of the Transition State Method to the Calculation of Reaction Velocities, Especially in Solution. *Trans. Faraday Soc.* **1935,** *31*, 875-894.
44. Gounder, R.; Iglesia, E., The Catalytic Diversity of Zeolites: Confinement and Solvation Effects within Voids of Molecular Dimensions. *Chem. Commun.* **2013,** *49* (34), 3491-3509.
45. Klisińska, A.; Samson, K.; Gressel, I.; Grzybowska, B., Effect of Additives on Properties of V_2O_5/SiO_2 and V_2O_5/MgO Catalysts: I. Oxidative Dehydrogenation of Propane and Ethane. *Appl. Catal., A* **2006,** *309* (1), 10-16.

Appendix

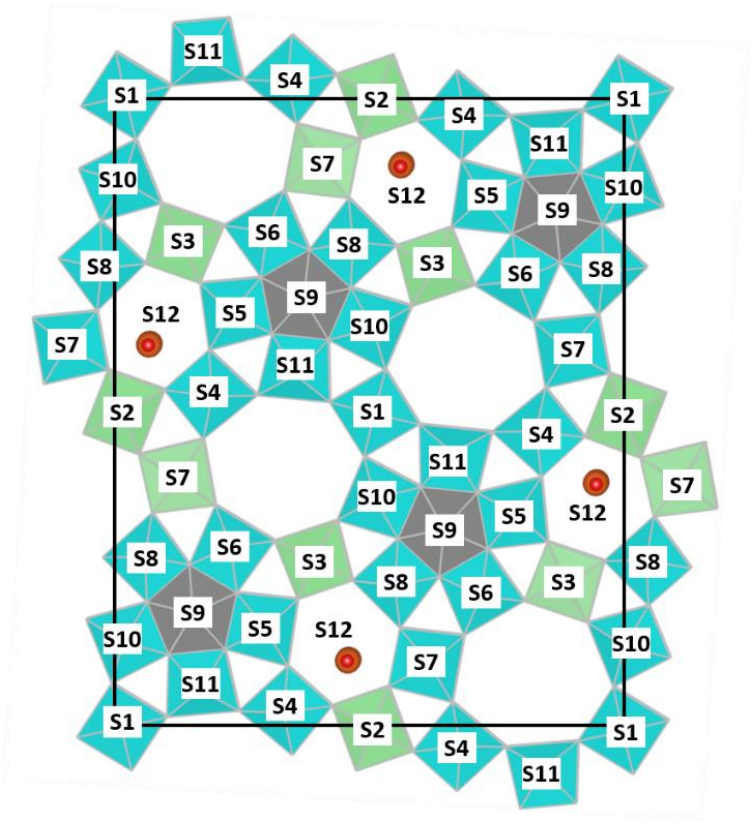

Scheme A1. A two dimensional polyhedral representation of the M1 phase of MoVTeNbO. Mo sites and V sites are shown as blue and green octahedra, respectively (S1-S8, S10, S11). Nb sites are shown as gray pentagonal bipyramids (S9). Te sites are shown as orange spheres (S12).

Table A1. MoVTeNbO synthesis parameters, and elemental composition

Parameters	Method 1 (This work)	Method 2 (Earlier work *insert publiatoion*)
Molar ratio of Mo/V/Te/Nb	1/0.25/0.23/0.12	1/0.25/0.17/0.12
Temperature	403 K	448 K
Time	96 h	48 h
Water	150 cm^3	75 cm^3
Volume of Teflon vessel	200 cm^3	100 cm^3
Product elemental composition	1/0.28/0.18/0.25	1/0.27/0.02/0.09
C_2H_6/C_6H_{12} ODH rate ratio*	0.507	1.09

*Reaction conditions: 648 K, 3 kPa C_2H_6 or C_6H_{12}, 3 kPa O_2, 30 cm^3 min^{-1}

Table A2. Rate and equilibrium constants from previous work[28] for C_2H_6 and C_6H_{12} ODH obtained by regression of measured rates to the form of Equations 5 and 6 on VO_x/SiO_2 and MoVTeNbO. Uncertainties represent two times the standard deviations.

Oxide	Temperature (K)	$k_{ODH}K_{ads}$ (10^{-5} $V^{-1}kPa^{-1}s^{-1}$)	K_{ads} (10^{-2} kPa^{-1})	k_5 (10^{-5} V^{-1} kPa^{-1} s^{-1})
		C_2H_6 ODH		
VO_x/SiO_2	648	0.062 (±0.003)	1.53 (±2.35)	0.21 (±0.06)
	673	0.098 (±0.005)	-2.16 (±2.62)	0.33 (±0.10
	698	0.193 (±0.012)	3.11 (±3.50)	0.57 (±0.20
	733	0.354 (±0.021)	1.33 (±3.27)	1.31 (±0.54
MoVTeNbO	648	3.87 (±0.27)	6.73 (±3.76)	52 (±90)
	673	6.46 (±0.06)	2.60 (±0.52)	208 (±119)
	698	11.7 (±0.2)	0.50 (±0.68)	353 (±249)
	733	24.0 (±0.6)	-0.83 (±1.23)	565 (±562)
		C_6H_{12} ODH		
VO_x/SiO_2	588	5.95 (±0.67)	14.4 (±6.4)	4.58 (±0.73)
	603	8.02 (±0.92)	23.1 (±7.0)	7.91 (±1.70)
	623	8.57 (±1.69)	11.2 (±10.7)	11.3 (±5.3)
	648	15.0 (±0.9)	10.9 (±4.7)	16.7 (±5.7)
MoVTeNbO	603	2.07 (±0.34)	11.1 (±9.2)	2.72 (±1.10)
	623	3.62 (±0.40)	9.04 (±6.13)	4.68 (±1.25)
	648	5.88 (±0.83)	5.79 (±7.75)	7.62 (±2.60)
	673	11.6 (±0.6)	3.94 (±2.76)	14.9 (±1.8)

DFT derived C-H bond dissociation energies for C_2H_6 and C_6H_{12}

C-H bond dissociation enthalpies are defined as the energy required for cleaving a C-H bond to form a fully relaxed isolated hydrocarbon radical and an isolated H-atom. These values were determined at standard conditions (1 atm pressure and 298.15 K) using Gaussian 09 program with B3LYP method and 6-31G(d,p) basis set. The calculated values for C_2H_6 and C_6H_{12} are shown in Table S6. All C-H bonds in these molecules are identical and will lead to the same dissociation enthalpy.

Table A3. C-H Bond dissociation enthalpies for C_2H_6 and C_6H_{12}.[28]

Molecule	C-H Bond dissociation enthalpy (kJ mol^{-1})
C_2H_6	408
C_6H_{12}	422

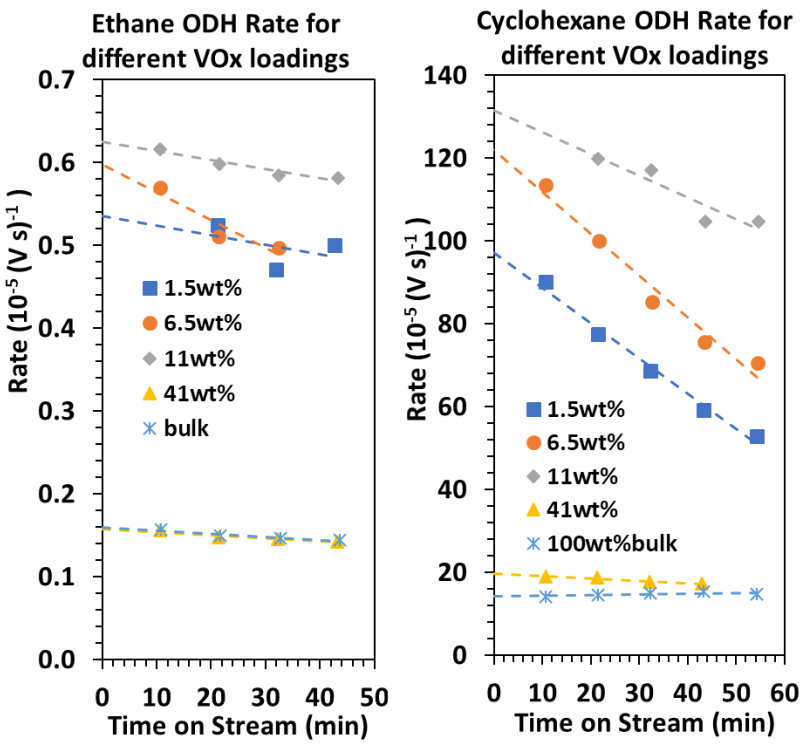

Figure A1: Measured C_2H_6 and C_6H_{12} rates on 1.5, 6.5, 11, 41wt% VO_x/SiO_2 and bulk V_2O_5, (648 K, 3 kPa C_2H_6 or C_6H_{12}, 3 kPa O_2, 30 cm^3 min^{-1}; Respective C_2H_6 conversions: 0.04%, 0.14%, 0.53%, 0.92% and 0.47%; Respective C_6H_{12} conversions 4%, 5%, 5%, 8%, 5%).

Influence of catalyst dilution on reaction rates

Rates of C_2H_6 and C_6H_{12} activation were measured at conversions below 10% on undiluted MoVTeNbO, MoVO and VO_x/SiO_2 samples and after dilution of these samples with nitric acid washed SiO_2. The diluted samples were prepared with 1:2 catalyst:diluent weight ratios with intimate mixing followed by pressing, crushing and sieving of powders to retain 106-180 μm aggregates. Figure A2 shows the measured rates on both oxides at identical conditions. The rates on diluted and undiluted VO_x/SiO_2 samples were nearly identical. The rates between undiluted and diluted MoVTeNbO samples were different by up to 20%, but they did not change in a systematic manner. For example, C_2H_6 rates increased with dilution, while C_6H_{12} rates decreased. These variations are much smaller than changes in rates expected in diffusion limited reactions. The small measured variations and their unsystematic nature suggests that mixing and pressing MoVTeNb samples caused small modifications to exposed external surfaces and pores, which led to inconsequential minor variations in rates.

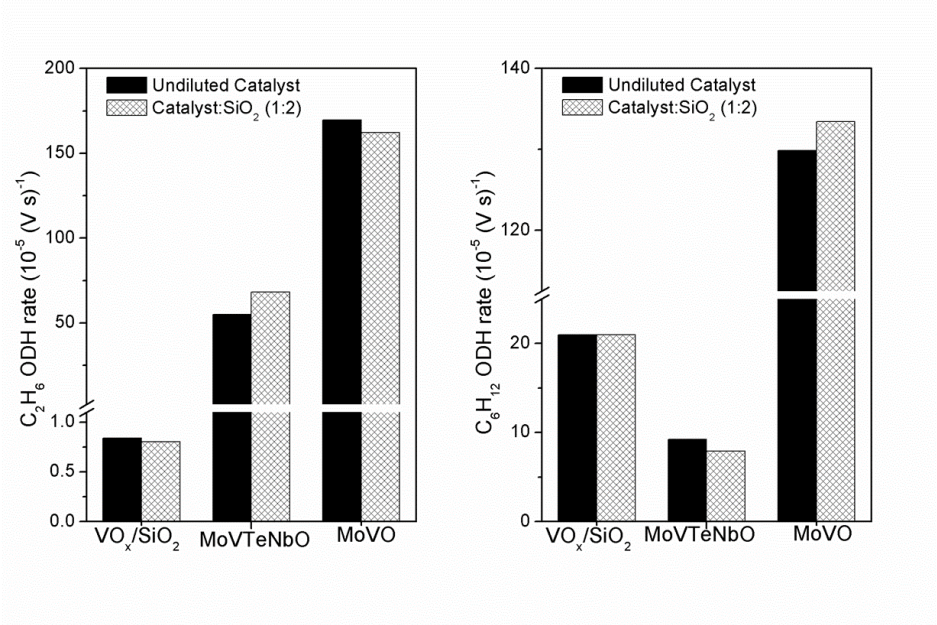

Figure A2. Measured (a) C_2H_6 and (b) C_6H_{12} ODH rates on 41 wt% VO_x/SiO_2, MoVTeNbO (different batch using synthesis method #2) and MoVO at 3 kPa C_2H_6 or C_6H_{12}, 3 kPa O_2, 30 cm^3 min^{-1} at 733 K (C_2H_6 on VO_x/SiO_2 and MoVTeNbO) and 648 K (C_2H_6 on MoVO, and C_6H_{12} on VO_x/SiO_2, MoVTeNbO and MoVO)

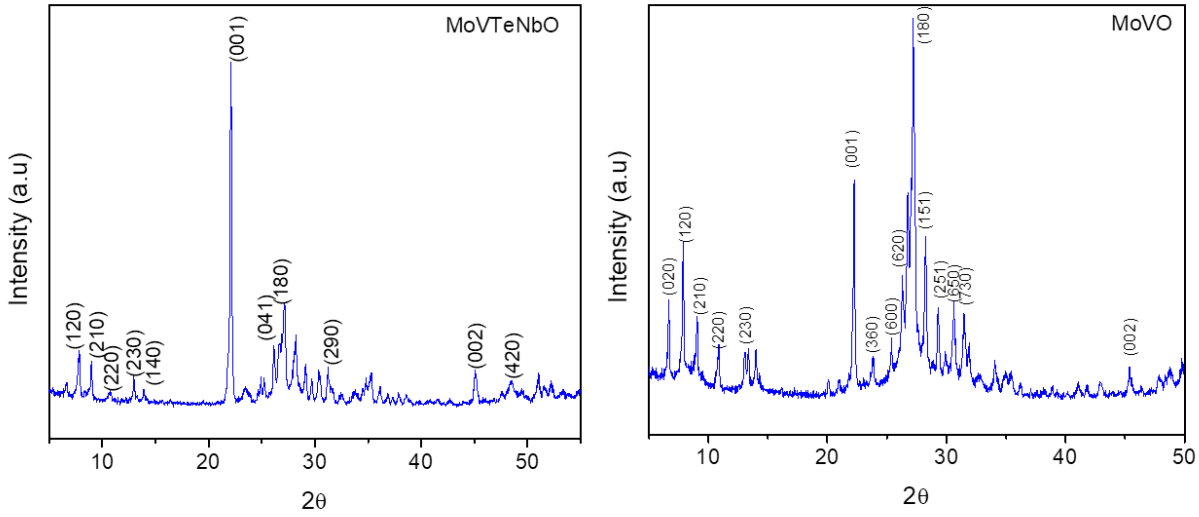

Figure A3: XRD pattern for ground (a) MoVTeNbO and (b) MoVO samples.

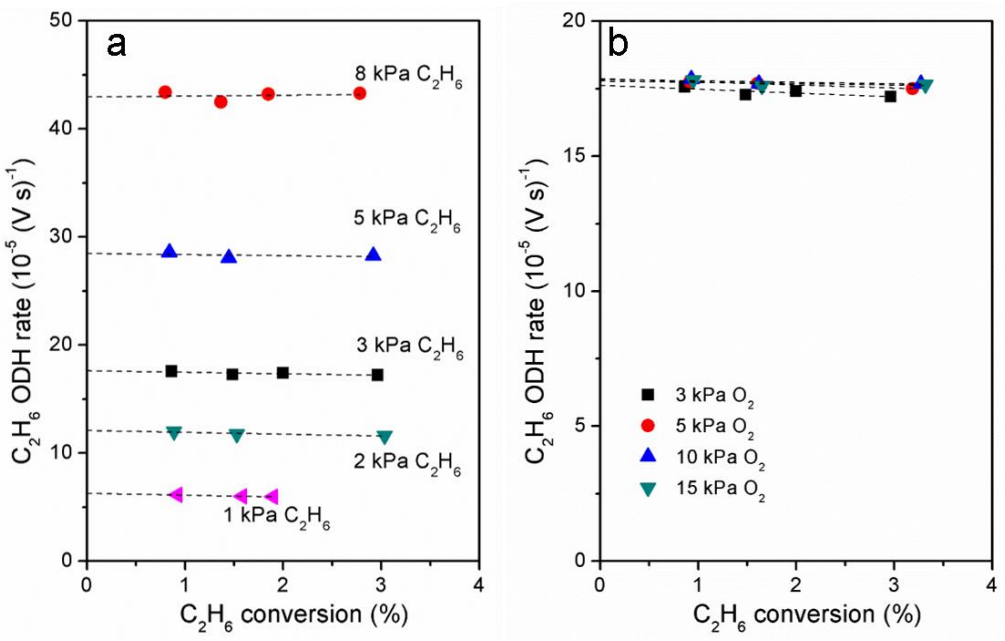

Figure A4. Measured C_2H_6 ODH rates (previous work) on MoVTeNbO as a function of C_2H_6 conversion at 673 K and (a) 1-8 kPa C_2H_6 and 3 kPa O_2, and (b) 3-15 kPa O_2 and 3 kPa C_2H_6. Dashed lines represent best linear regression fits.[28]

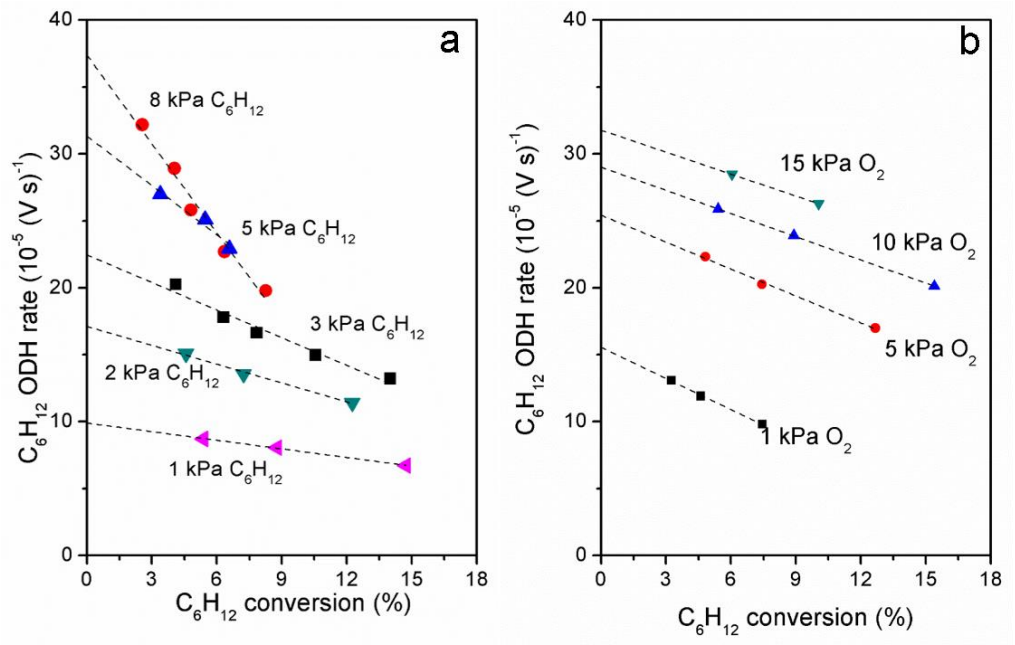

Figure A5. Measured C_6H_{12} ODH rates (previous work) on MoVTeNbO as a function of C_6H_{12} conversion at 673 K and (a) 1-8 kPa C_6H_{12} and 3 kPa O_2, and (b) 1-15 kPa O_2 and 3 kPa C_6H_{12}. Dashed lines represent best linear regression fits.[28]

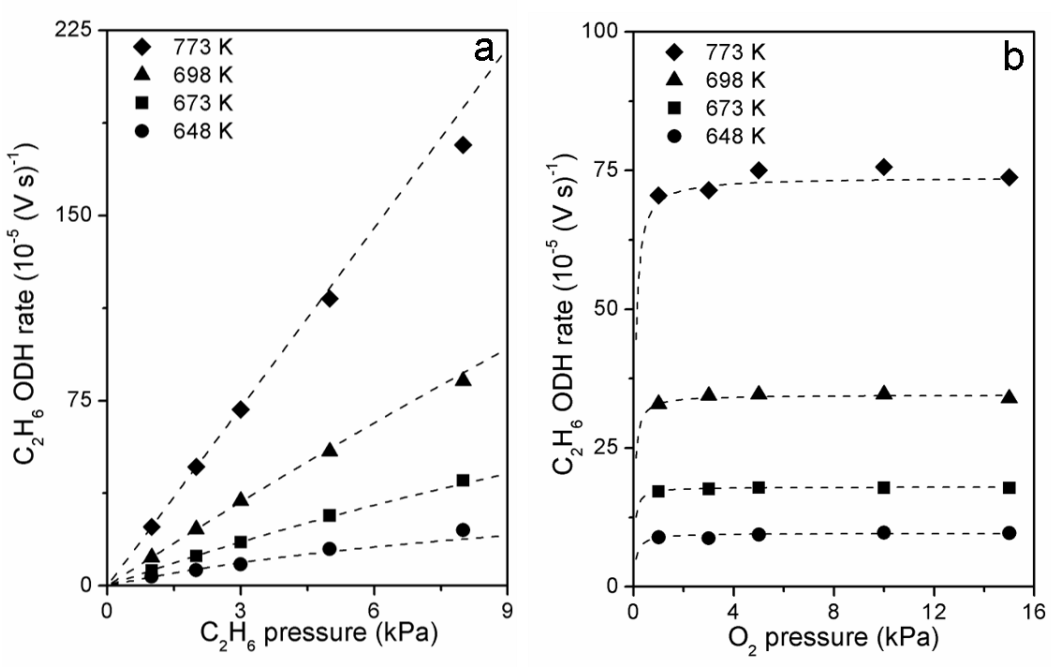

Figure A6. Measured C_2H_6 ODH rates (previous work) on MoVTeNbO as a function of (a) C_2H_6 pressure at 3 kPa O_2 and (b) O_2 pressure at 3 kPa C_2H_6. Rates were extrapolated to zero conversion using linear fits to the effect of conversion on rates. Dashed curves represent best regression fits to the form Equation 5.[28]

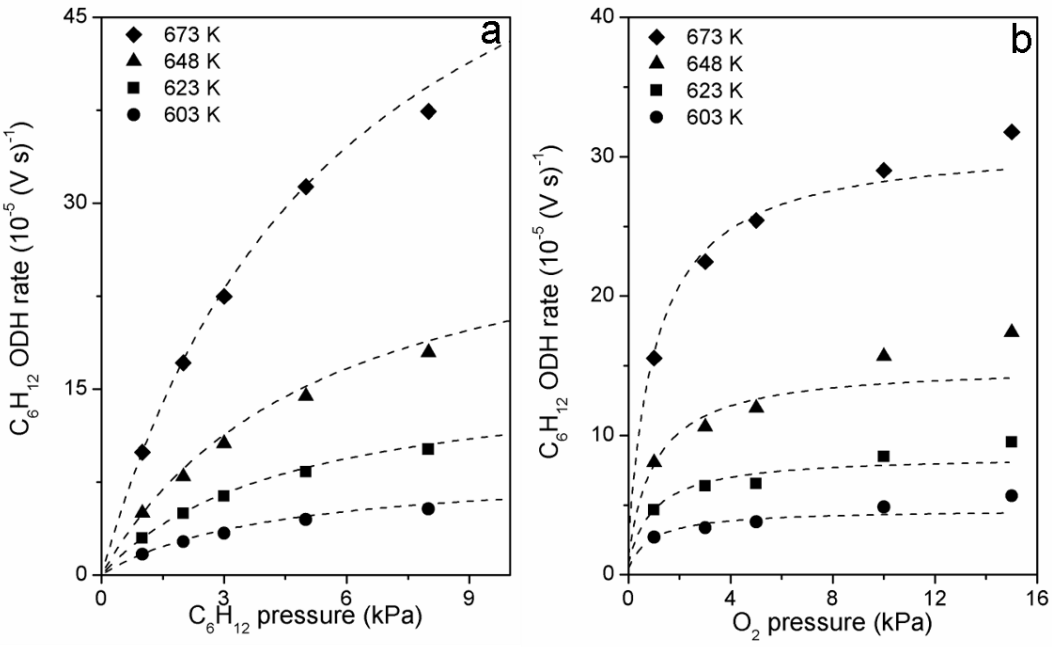

Figure A7. Measured C_6H_{12} ODH rates (previous work) on MoVTeNbO as a function of (a) C_6H_{12} pressure at 3 kPa O_2 and (b) O_2 pressure at 3 kPa C_6H_{12}. Rates were extrapolated to zero conversion using linear fits to the effect of conversion on rates. Dashed curves represent best regression fits to the form Equation 6.[28]

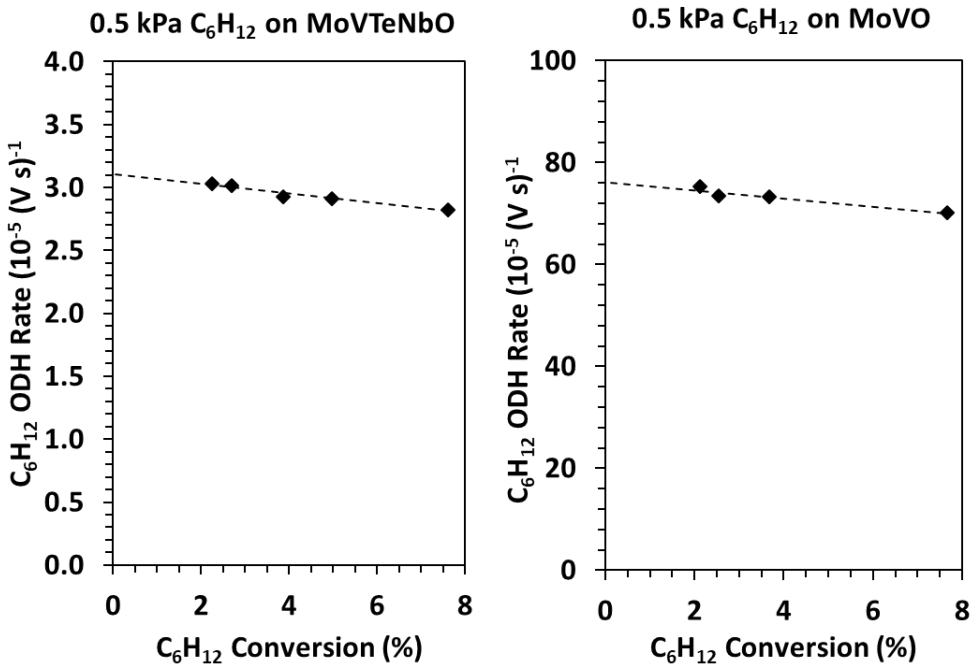

Figure A8. Measured C_6H_{12} ODH rates (this work) on (a) MoVTeNbO and (b) MoVO as a function of C_6H_{12} conversion at 648 K and 0.5 kPa C_6H_{12} and 3 kPa O_2. Different conversions achieved by varying flow rates between 30–105 cm^3/min Dashed lines represent best linear regression fits.

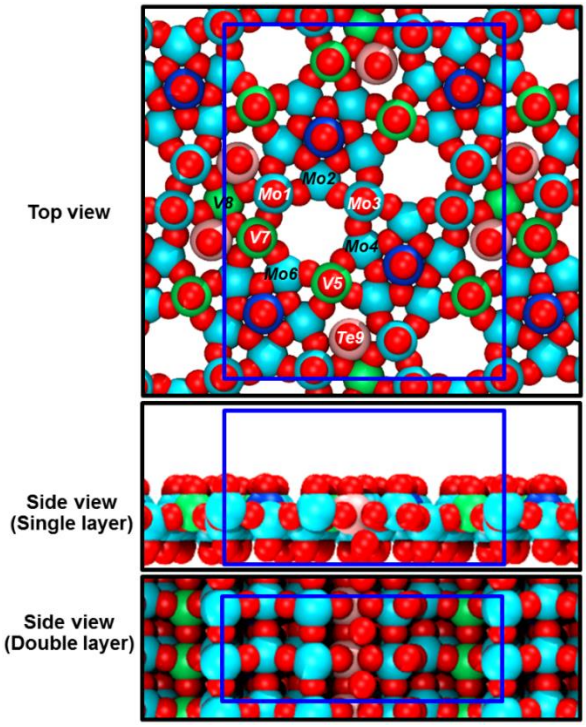

Figure A9. Structure models (a) bulk MoVTeNbO ($Mo_{56}V_{16}Te_8Nb_8O_{232}$), and (b) single layer MoVTeNbO exposing external surfaces ($Mo_{28}V_8Te_4Nb_4O_{116}$). Blue rectangles represent periodic supercell boundaries. V-atoms occupy S2, S3 and half of S7 sites shown in Scheme A1.

Calculation of Micropore wall areas and external surface area

Micropore wall area: Micropores are assumed to be cylinders of radius, r = 0.2 nm which leads to the following relation between the micropore wall area (A_{micro}) and the volume:

$$\frac{A_{micro}}{V_{micro}} = \frac{2\pi rL}{\pi r^2 L} = \frac{2}{r}\,;\, A_{micro} = \frac{2V_{micro}}{r} \quad \text{(A1)}$$

where, L is the total length of the micropores.

External area: The nitrogen uptake volumes (V) between relative pressures (P/P_0 values) 0.05 and 0.35 were used to plot $\frac{1}{\mathrm{V}((P_0/P)-1)}$ values as a function of $\frac{P}{P_0}$, in which a linear regression was used to obtain the slope and an intercept described by the Brunauer-Emmett-Teller (BET) equation:

$$\frac{1}{\mathrm{V}((P_0/P)-1)} = \frac{1}{\mathrm{V_m}C} + \frac{C-1}{\mathrm{V_m}C}\left(\frac{P}{P_0}\right) \quad \text{(A2)}$$

where, V_m is the volume of adsorbates constituting a monolayer of surface coverage, and C in the BET constant. The V_m value determined from the regression is related to the surface area (S) according to:

$$S = \frac{V_m N_A A_{cs}}{V} \quad \text{(A3)}$$

where, V is the molar volume of N_2 at STP, N is the Avogadro number, A_{cs} is the molecular cross section al area of N_2 (16 Å^2).

Definitions of conversion and selectivity

C_2H_6 and C_6H_{12} conversions (X) and selectivity (S) to products in oxidative reactions were calculated from molar concentrations in reactor effluents (C)

$$X_{\mathrm{C_2H_6}} = \frac{C_{\mathrm{C_2H_4}} + C_{\mathrm{CH_3CHO}} + \frac{1}{2}C_{\mathrm{CO}} + \frac{1}{2}C_{\mathrm{CO_2}}}{C_{\mathrm{C_2H_6}} + C_{\mathrm{C_2H_4}} + C_{\mathrm{CH_3CHO}} + \frac{1}{2}C_{\mathrm{CO}} + \frac{1}{2}C_{\mathrm{CO_2}}} \times 100\ \% \quad \text{(A4)}$$

$$X_{\mathrm{C_6H_{12}}} = \frac{C_{\mathrm{C_6H_{10}}} + C_{\mathrm{C_6H_6}} + C_{\mathrm{C_6H_{10}O}} + C_{\mathrm{C_6H_{10}O_4}} + \frac{1}{6}C_{\mathrm{CO}} + \frac{1}{6}C_{\mathrm{CO_2}}}{C_{\mathrm{C_6H_{12}}} + C_{\mathrm{C_6H_{10}}} + C_{\mathrm{C_6H_6}} + C_{\mathrm{C_6H_{10}O}} + C_{\mathrm{C_6H_{10}O_4}} + \frac{1}{6}C_{\mathrm{CO}} + \frac{1}{6}C_{\mathrm{CO_2}}} \times 100\ \% \quad \text{(A5)}$$

$$S_k = \frac{x_k \times C_k}{\sum_{k=1}^{n}(x_k \times C_k)} \times 100\ \% \quad \text{(A6)}$$

where, x_k is the number of carbon atoms in a given product and n is the total number of products.